NUMERICAL SOLUTION OF THE EULER EQUATION FOR COMPRESSIBLE INVISCID FLUIDS

by

Antony Jameson
Princeton University
Princeton, New Jersey U.S.A.

Report MAE 1643

"NUMERICAL SOLUTION OF THE EULER EQUATION FOR COMPRESSIBLE INVISCID FLUIDS"

by

Antony Jameson
Department of Mechanical and Aerospace Engineering
Princeton University
Princeton, New Jersey 08544
U.S.A.

* * * *

Text for Meeting of the

Institut National De Recherche
En Informatique Et En Automatique
Euler Workshop
December 7-9, 1983
FRANCE

1. Objective and Guiding Principles

The objective of this work is to develop a satisfactory numerical method for the calculation of steady solutions of the Euler equations for inviscid compressible gas flows. The intended application is the prediction of the aerodynamic properties of airplanes flying at transonic speeds. This will ulimately call for solutions of the viscous equations. The Reynolds numbers prevailing in full scale flight are typically very large, with the result that the boundary layers become turbulent, forcing recourse to statistical averaging and the introduction of turbulence models. We may regard the solution of the Euler equations as a way station on the route to this longer term objective. My emphasis is on steady flow.

Some of the principal difficulties of the problem are:

(1) The equations of gas dynamics are nonlinear.

(2) Solutions in the transonic range will ordinarily be discontinuous: Cathleen Morawetz has shown that shock free solutions are isolated points [1]. Thus we may expect to find shock waves. The solutions will also generally contain contact surfaces in the form of vortex sheets (shed both by wings in three-dimensional flow, and also by profiles in two-dimensional flow in the event that shock waves of differing strength produce different amounts of entropy on the upper and lower surfaces).

(3) There are regions of the flow in the neighborhood, for example, of stagnation points, the wing trailing edge

or the wing tip, where the derivatives may become very large or even unbounded, leading to large discretization errors.

(4) The equations are to be solved in an unbounded domain.

(5) We are generally interested in calculating flows over bodies of extreme geometric complexity (including cases where the domain is multiply connected).

In order to find one's way through this thicket of difficulties and pitfalls, Peter Lax has suggested the need for "design principles" to guide the construction of a numerical scheme appropriate to the problem*. The present work follows the general plan of attack which I proposed in 1981 [2]. A steady solution is obtained as the asymptotic state of a time dependent problem. Since the unsteady problem is used only as a vehicle for reaching the steady state, alternative iterative schemes might be comtemplated. An example is the least squares method, which has reached a high level of sophistication at the hands of Glowinski and his co-workers [3]. I believe, however, that the time marching formulation is worth considering for some of the following reasons:

(1) Its simplicity (with consequent reduction of the risk of programming error).

---

*Baejter Seminar, Princeton, October 1983

(2) It offers the possibility of providing a dual purpose computer program for both steady and unsteady problems.

(3) Where there is a possibility of a non-unique steady state or perhaps a non-physical solution, containing, for example, a discontinuous expansion, one may rely on the modeling of a true physical process to make an appropriate selection.

(4) Algorithms can rather easily be devised which take maximum advantage of vector computers.

None of these virtues could be considered decisive if the convergence of the time marching scheme to a steady state were excessively slow in comparison with competing methods. I hope to show, however, that the time marching method can be modified in such a way that this need not be the case.

Within the framework of the time marching formulation the design principles which have guided this work are:

(1) The conservation laws of gas dynamics will be satisfied in discrete conservation form by the numerical approximation. (We may then rely on the theorem of Lax and Wendroff that the correct shock jump conditions will be satisfied by the solution if it converges in the limit of decreasing mesh width [4]).

(2) Unphysical solutions are to be excluded by the introduction of appropriate dissipative terms in the discrete approximation.

(3) The final steady state should be independent of the time marching procedure. (I do not wish to exclude the possibility that the

final steady state will depend on the initial state, although there is evidence provided by numerous flying objects suggesting the repeatability of a substantial class of steady solutions). This requirement does, however, exclude the use of a number of popular difference schemes, including schemes with fractional steps, and the Lax Wendroff and MacCormack schemes.

(4) If a quantity is known to be invariant in the true solution, it should also be invariant in the numerical solution. In particular, the total enthalpy should be constant in the steady state solution.

(5) Uniform flow should be an exact solution of the difference equations on an arbitrary mesh.

In order to meet requirement (3) I believe that it is helpful to separate the space discretization procedure entirely from the time marching procedure by applying first a semi-discretization. This has the advantage of allowing the problems of spatial discretization error, artificial dissipation and shock modeling to be studied independently of the problems of time marching stability and convergence acceleration. I believe that my own studies of convergence acceleration procedures will be found to be essentially complementary to the large body of recent work that has been devoted to improving the modeling of shock waves and contact discontinuties.

The main measures for accelerating the convergence to steady state which have been applied in this work are:

(1) Modification of the differential equations for faster convergence to a steady state.

(2) The use of a hybrid multistage time stepping scheme with distinct and separately optimized treatment of the hyperbolic and parabolic terms.

(3) The use of residual averaging to permit a larger time step without violating stability restrictions.

(4) Parallel time stepping on multiple grids.

The use of all these measures in conjunction has made it possible to obtain satisfactory solutions of the Euler equations for two dimensional flows in 25-50 steps.

Since I first proposed the use of multistage time stepping schemes for solving the Euler equations [2], numerous modifications of both the time stepping and space discretization schemes have been introduced, and the treatment of the boundary condition has also been altered. In this text I therefore describe the entire scheme as it now stands. Modifications of the Euler equations for faster convergence to a steady state are reviewed in the next section. Section 3 discusses the spatial discretization scheme which is derived from the integral form of the conservation laws. Section 4 discusses a relatively simple form of adaptive dissipation which leads to reasonably satisfactory modeling of shock waves in steady flows. The following section discusses schemes designed to improve shock resolution. These rely on more complicated constructions of artificial dissipation based on the concept of diminishing total variation for scalar conservation laws, following the ideas of Lax, Harten, van Leer and Osher [5,6]. In the light of this discussion it can be seen that the adaptive dissipation can be designed to yield a scheme which

locally behaves like a TVD scheme in the neighborhood of a shock wave. The optimal construction, however, requires a decomposition into characteristic fields along the lines proposed by Roe [7,8]. Section 6 reviews the treatment of boundary conditions. Section 7 presents a class of hybrid multi-stage time stepping schemes, while Sections 8 and 9 review the residual averaging and multiple grid schemes. In order to test the various ingredients in a less complex setting, Section 10 presents some results of tests with Burger's equation. Section 11 presents some representative results for the Euler equations.

2. Modification of the Equations to Improve Convergence to a Steady State

The motion of an inviscid compressible gas is governed by the Euler equations. Let p, ρ, u, v, E, H and c denote the pressure, density, Cartesian velocity components, total energy, total enthalpy and speed of sound. For a perfect gas

$$E = \frac{p}{(\gamma-1)\rho} + \frac{1}{2}(u^2 + v^2), \quad H = E + \frac{p}{\rho} \tag{2.1}$$

$$c^2 = \frac{\gamma p}{\rho}$$

where γ is the ratio of specific heats. Using Cartesian space coordinates x and y, the Euler equations for a two dimensional time dependent flow are

$$\frac{\partial w}{\partial t} + \frac{\partial}{\partial x} f(w) + \frac{\partial}{\partial y} g(w) = 0 \tag{2.2}$$

where t is the time coordinate and

$$w = \begin{bmatrix} \rho \\ \rho u \\ \rho v \\ \rho E \end{bmatrix}, \qquad f = \begin{bmatrix} \rho u \\ \rho u^2 + p \\ \rho uv \\ \rho uH \end{bmatrix}, \qquad g = \begin{bmatrix} \rho v \\ \rho vu \\ \rho v^2 + p \\ \rho vH \end{bmatrix} \tag{2.3}$$

These equations are to be solved for a steady state $\frac{\partial w}{\partial t} = 0$.

Aside from trying to construct the most efficient possible numerical method, it is natural to consider the possibility of modifying the Euler equations to improve the rate of convergence to a steady state. Three main approaches have been tried in this work.

The first is to use locally varying time steps such that the difference scheme operates everywhere in the flow field close to its stability limit. This is equivalent to solving

$$\frac{\partial w}{\partial t} + \alpha\left\{ \frac{\partial}{\partial x} f(w) + \frac{\partial}{\partial y} g(w)\right\} = 0 \qquad (2.4)$$

where α is a variable scaling factor. This method ensures that disturbances will be propagated to the outer boundary in a fixed number of steps, proportional to the number of mesh intervals between the body and the outer boundary.

The second approach is based on the observation that if the enthalpy has a constant value H_∞ in the far field, it is constant everywhere in a steady flow, as can be seen by comparing the equations for conservation of mass and energy. If we set $H = H_\infty$ everywhere in the flow field throughout the evolution, then the pressure can be calculated from the equation

$$p = \frac{\gamma-1}{\gamma} \rho \left(H_\infty - \frac{u^2+v^2}{2}\right)$$

This eliminates the need to integrate the energy equation. The resulting three equation model still constitutes a hyperbolic system, which approaches the same steady state as the original system. The use of this model has been advocated by Veuillot and Viviand [9].

The third approach is to retain the energy equation, and to add forcing terms proportional to the difference between H and H_∞ [10]. In a subsonic irrotational flow one can introduce a velocity potential ϕ and set

$$u = \phi_x \quad , \quad v = \phi_y \ .$$

The Euler equations then reduce to the unsteady potential flow equation

$$\phi_{tt} + 2u\phi_{xt} + 2v\phi_{yt}$$

$$= (c^2 - u^2)\,\phi_{xx} - 2uv\phi_{xy} + (c^2 - v^2)\phi_{yy} \qquad (2.6)$$

This is simply the equation for undamped wave motion in a moving coordinate frame. Damping could be introduced by adding a term $\alpha\phi_t$ to this equation. Such a term cannot directly be added to the Euler equations. However, the Bernoulli equation for unsteady potential flow is

$$\phi_t + H = H_\infty$$

Thus one can simulate the addition of a term $\alpha\phi_t$ to (2.6) by adding terms proportional to $H-H_\infty$ to the Euler equations. Provided that the space discretization scheme is constructed in such a way that $H = H_\infty$ is consistent with the steady state solution of the difference equations, these terms do not alter the final steady state. Numerical experiments have confirmed that they do assist convergence. The terms added to the mass and momentum equations are $\alpha\rho(H-H_\infty)$, $\alpha\rho u(H-H_\infty)$ and $\alpha\rho v(H-H_\infty)$, while that added to the energy equation is $\alpha\rho(H-H_\infty)$. In calculations using multiple grids an effective strategy is to include these terms only on the fine grid, and to increase the parameter α.

3. Finite Volume Formulation

The space discretization scheme is developed by writing the Euler equations in integral form

$$\frac{\partial}{\partial t} \iint_S w dS + \int_{\partial S} (f dy - g dx) = 0 \tag{3.1}$$

for a domain S with boundary ∂S. The computational domain is divided into quadrilateral cells denoted by the subscripts i,j as sketched in Figure 1. Assuming that the dependent variables are known at the center of each cell, a system of ordinary differential equations is obtained by applying equation (3.1) separately to each cell. These have the form

$$\frac{d}{dt} (S_{i,j} w_{i,j}) + Q_{i,j} = 0 \tag{3.2}$$

where $S_{i,j}$ is the cell area, and $Q_{i,j}$ is the net flux out of the cell. This may be evaluated as

$$\sum_{k=1}^{4} (\Delta y_k f_k - \Delta x_k q_k) \tag{3.3}$$

where f_k and g_k denote values of the flux vectors f and g on the k^{th} edge, Δx_k and Δy_k are the increments of x and y along the edge with appropriate signs, and the sum is over the four sides of the cell. The flux vectors are evaluated by taking the average of the values in the cells on either side of each edge. For example

$$f_2 = \frac{1}{2} (f_{i+i,j} + f_{i,j}) \tag{3.4}$$

where $f_{i,j}$ denotes $f(w_{i,j})$. Alternatively one may evaluate first the flux velocity

$$Q_k = \frac{\Delta y_k (\rho u)_k - \Delta x_k (\rho u)_k}{\rho_k}$$

on each edge. Then the flux for the x momentum component, for example, is

$$\sum_{k=1}^{4} \{Q_k(\rho u)_k + \Delta y_k \, p_k\} \tag{3.5}$$

Schemes constructed in this manner reduce to central difference schemes on Cartesian meshes, and are second order accurate if the mesh is sufficiently smooth. They also satisfy the design principle (5) that uniform flow should be an exact solution of the difference equations. Provided that they are augmented by appropriate dissipative terms, they have been found to give quite accurate results, and they can easily be extended to three dimensional flows [11,12].

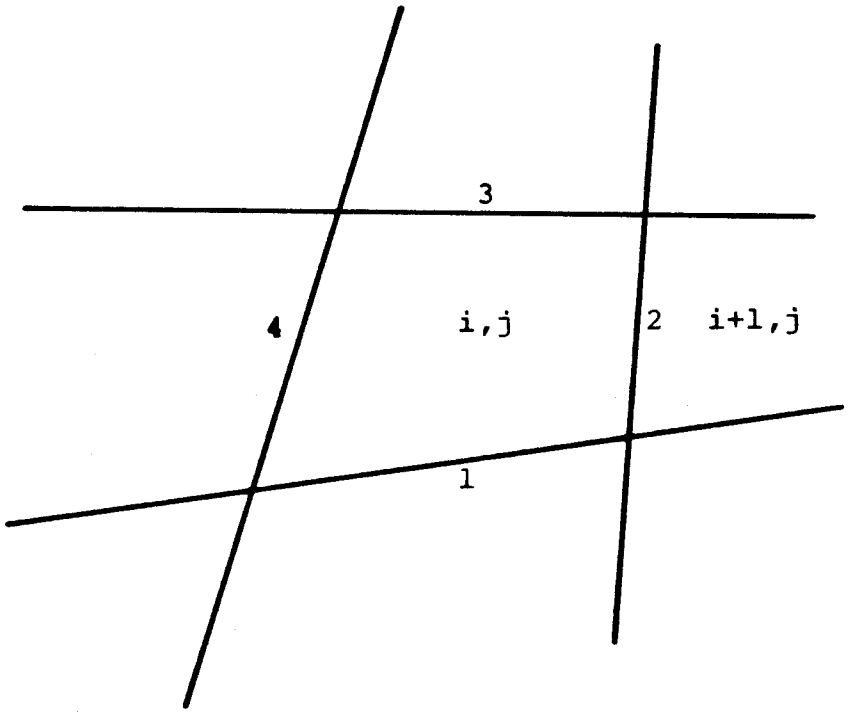

Figure 1

Finite Volume Scheme

4. Adaptive Dissipation

The finite volume scheme (3.2) is not dissipative, allowing undamped oscillations with alternate sign at odd and even mesh points. In order to eliminate spurious oscillations, which will be triggered by discontinuities in the solution, one can follow either of two strategies. The first is to begin with a non-dissipative scheme such as (3.2), or a fourth order scheme, and to add just enough dissipation where it is needed to control the tendency to produce spurious oscillations. The second approach, which can be traced to the work of Boris, Book and Zalesak [13,14], is to begin by adding enough dissipation everywhere to guarantee the absence of unwanted oscillations. This leads to a first order accurate scheme which excessively smears discontinuities. A correction is then added to cancel the first order error, but the correction is limited to prevent the introduction of overshoots near discontinuities. This idea is the basis of an ingenious method recently proposed by Harten [15] for the construction of schemes which promise to give sharp resolution of shock waves. In this section I describe an adaptive scheme for adding dissipation which has proved effective in practice, and in the next section, I shall consider the more complex high resolution schemes. The idea of the adaptive scheme is to add third order dissipative terms throughout the domain to provide a base level of dissipation sufficient to prevent nonlinear instability, but not sufficient to prevent oscillations in the neighborhood of shock waves. In order to capture shock waves additional first order dissipative terms are added locally by a sensor designed to detect discontinuities.

With the addition of dissipative terms $D_{i,j}$, the semi-discrete equations (3.2) take the form

$$\frac{d}{dt}\,(S_{i,j}\,w_{i,j}) + Q_{i,j} - D_{i,j} = 0 \quad . \tag{4.1}$$

To preserve conservation form the dissipative terms are generated by dissipative fluxes. The dissipation for the density equation, for example, is

$$D_{i,j}(\rho) = d_{i+1/2,j} - d_{i-1/2,j} + d_{i,j+1/2} - d_{i,j-1/2} \tag{4.2}$$

where the dissipative flux $d_{i+1/2,j}$ is defined by

$$\begin{aligned} d_{i+1/2,j} = {} & \varepsilon^{(2)}_{i+1/2,j}\, R_{i+1/2,j}\, (\rho_{i,j} - \rho_{i-1,j}) \\ & - \varepsilon^{(4)}_{i+1/2,j}\, R_{i+1/2,j}\, (\rho_{i+2,j} - 3\rho_{i+1,j} + 3\rho_{i,j} - \rho_{i-1,j}) \quad . \end{aligned} \tag{4.3}$$

Here $\varepsilon^{(2)}_{i+1/2,j}$ and $\varepsilon^{(4)}_{i+1/2,j}$ are adaptive coefficients, and $R_{i+1/2,j}$ is a coefficient chosen to give the dissipative terms the proper scale. An appropriate scaling factor is

$$R_{i+1/2,j} = \lambda_{i+1/2,j} \tag{4.4}$$

where λ is the spectral radius of the Jacobian matrix

$$\Delta y \frac{\partial f}{\partial w} - \Delta x \frac{\partial g}{\partial w}$$

for the flux across the cell face. This can be estimated as

$$\lambda = |\Delta y\, u - \Delta x\, v| + c\,\sqrt{\Delta x^2 + \Delta y^2} \tag{4.5}$$

where c is the speed of sound, and Δx and Δy are the displacements of the face in the x and y directions.

If one is using an explicit time stepping scheme one needs an estimate of the time step limit. A conservative estimate for a nominal Courant number of unity is

$$\Delta t^*_{i,j} = \frac{S_{i,j}}{\lambda_{i,j} + \mu_{i,j}}$$

where $\lambda_{i,j}$ and $\mu_{i,j}$ are the average spectral radii of the Jacobian matrices in the i and j directions. It is then convenient to avoid duplicate calculations by taking

$$R_{i+1/2,j} = \frac{1}{2}\left(\frac{S_{i+1,j}}{\Delta t^*_{i+1,j}} + \frac{S_{i,j}}{\Delta t^*_{i,j}}\right) \qquad (4.4^*)$$

An effective sensor of the presence of a shock wave can be constructed by taking the second difference of the pressure. Define

$$\nu_{i,j} = \left|\frac{p_{i+1,j} - 2p_{i,j} + p_{i-1,j}}{p_{i+1,j} + 2p_{i,j} + p_{i-1,j}}\right| \qquad (4.6)$$

Set

$$\bar{\nu}_{i+1/2,j} = \max\left(\nu_{i+2,j}, \nu_{i+1,j}, \nu_{i,j}, \nu_{i-1,j}\right)$$

Then we take

$$\varepsilon^{(2)}_{i+1/2,k} = \min\left(\frac{1}{2}, k^{(2)}\,\bar{\nu}_{i+1/2,j}\right)$$

and (4.7)

$$\varepsilon^{(4)}_{i+1/2,j} = \max\left(0, k^{(4)} - \alpha\,\bar{\nu}_{i+1/2,j}\right)$$

where $k^{(2)}$, $k^{(4)}$ and α are constants. Typically,

$$k^{(2)} = 1, \quad k^{(4)} = 1/32 , \quad \alpha = 2.$$

In a smooth region of the flow $\nu_{i,j}$ is proportional to the square of the mesh width, with the result that $\varepsilon^{(2)}_{i+1/2,j}$ is also proportional to the square of the mesh width, while $\varepsilon^{(4)}_{i+1/2,j}$ is of order one, and the dissipative fluxes are of third order in comparison with the convective fluxes. In the neighborhood of a shock wave $\nu_{i,j}$ is of order 1, so that the scheme behaves locally like a first order scheme. The term $\alpha\ \bar{\nu}^{(4)}_{i+1/2,j}$ is subtracted from $k^{(4)}$ to cut off the fourth differences which would otherwise cause an oscillation in the neighborhood of the shock wave.

The dissipative terms for the momentum and energy equations are constructed in the same way as those for the mass equation, substituting ρu, ρv or ρH for ρ in equation (4.3). The purpose of using differences of ρH rather than ρE in the dissipative terms for the energy equation is to produce difference equations which admit the solution $H = H_\infty$ in the steady state. With this choice the energy equation reduces to the mass equation multiplied by H_∞ when the time derivatives vanish.

5. Schemes Designed to Improve the Resolution of Shock Waves

There is by now a rather extensive theory of difference schemes for the treatment of a scalar conservation law

$$\frac{\partial u}{\partial f} + \frac{\partial}{\partial x} f(u) = 0 \tag{5.1}$$

This theory stems from the mathematical theory of shock waves, as it has been formulated by Lax [16]. It is known that the total variation

$$TV = \int_{-\infty}^{\infty} \left|\frac{\partial u}{\partial x}\right| dx$$

of a solution of (5.1) can never increase. Correspondingly it seems desirable that the discrete total variation

$$TV = \sum_{i=-\infty}^{\infty} |u_{i+1} - u_i|$$

of a solution of a difference approximation to (5.1) should not increase. A semi-discretization will have this property (now generally called total variation diminishing or TVD) if it can be cast in the form

$$\frac{du_i}{dt} = c^{+}_{i+1/2}(u_{i+1} - u_i) - c^{-}_{i-1/2}(u_i - u_{i-1}) \tag{5.2}$$

where the coefficients $c^{+}_{i+1/2}$ and $c^{-}_{i-1/2}$ are non-negative [17,18].

This can be proved as follows. The total variation can be expressed as

$$TV = \sum_{i=\infty}^{\infty} s_{i+1/2}\,(u_{i+1} - u_i)$$

where

$$s_{i+1/2} = \begin{cases} 1 \text{ if } u_{i+1} - u_i \geq 0 \\ -1 \text{ if } u_{i+1} - u_i < 0 \end{cases}$$

Thus

$$\frac{d}{dt} TV = \sum_{i=-\infty}^{\infty} s_{i+1/2} \frac{d}{dt} (u_{i+1} - u_i)$$

$$= \sum_{i=-\infty}^{\infty} s_{i+1/2} \{c^+_{i+3/2}(u_{i+2} - u_{i+1})$$

$$-(c^+_{i+1/2} + c^-_{i+1/2})(u_{i+1} - u_i)$$

$$+ c^-_{i-1/2}(u_i - u_{i-1})\}$$

$$= - \sum_{i=-\infty}^{\infty} v_{i+1/2}(u_{i+1} - u_i)$$

where

$$v_{i+1/2} = (c^+_{i+1/2} + c^-_{i+1/2})\, s_{i+1/2}$$

$$- c^+_{i+1/2}\, s_{i-1/2} - c^-_{i+1/2}\, s_{i+3/2}$$

If $c^+_{i+1/2}$ and $c^-_{i+1/2}$ are non-negative it follows that $v_{i+1/2}$ is either zero, or else it has the same sign as $u_{i+1} - u_i$. Hence

$$\frac{d}{dt} TV \leq 0 .$$

This is a special case of a more general result for multi-point schemes [17].

Since the total variation will increase if an initially monotone profile ceases to be monotone, TVD schemes preserve monotonicity. The TVD property does not, however, guarantee fulfilment of the entropy condition that the only admissable discontinuous solutions are those for which the characteristics of (5.1) converge on the discontinuities from both sides [16]. Some TVD schemes admit stationary expansion shock waves, for example. Monotone time stepping schemes of the form

$$u_i^{n+1} = H(u_{i-\ell}^n, u_{i-\ell+1}^n, \cdots, u_{i+\ell}^n)$$

where

$$\frac{\partial H}{\partial u_\alpha} \geq 0 \qquad \text{for all } \alpha$$

are known to exclude entropy violating solutions [18, 19, 20]. Recently Osher has shown that semi-discrete approximations to (5.1) of the form

$$\frac{du_i}{dt} + \frac{1}{\Delta x}(h_{i+1/2} - h_{i-1/2}) = 0 \tag{5.3}$$

exclude entropy violating solutions if the numerical flux $h_{i+1/2}$ satisfies the condition

$$\text{sgn}(u_{i+1} - u_i)(h_{i+1/2} - f(u)) \leq 0$$

for all u between u_i and u_{i+1}. Osher calls schemes which satisfy this condition E schemes [18].

It can be shown that monotone and E schemes are at best first order accurate [18,19]. Harten devised a method of constructing TVD schemes which are second order accurate almost everywhere [15]. His construction can be adapted to a semi-discrete scheme as follows. Denoting $f(u_i)$ by f_i, define the numerical flux in equation (5.3) as

$$h_{i+1/2} = \frac{1}{2}\ (f_{i+1} + f_i) - \alpha_{i+1/2}(u_{i+1} - u_i)\ . \tag{5.4}$$

Now suppose that

$$\alpha_{i+1/2} = \frac{1}{2}\ k|a_{i+1/2}| \tag{5.5}$$

where

$$a_{i+1/2} = \begin{cases} \dfrac{f_{i+1}-f_i}{u_{i+1}-u_i} & \text{if } u_{i+1} \neq u_i \\ \dfrac{\partial f}{\partial u}\Big|_{u=u_i} & \text{if } u_{i+1} = u_i \end{cases}\ . \tag{5.6}$$

Then it follows that

$$h_{i+1/2} = f_i - \frac{1}{2}\ (k|a_{i+1/2}| - a_{i+1/2})\ (u_{i+1} - u_i)$$

and

$$h_{i-1/2} = f_i - \frac{1}{2}\ (k|a_{i-1/2}| + a_{i-1/2})\ (u_i - u_{i-1}).$$

This gives (5.2) with

$$c^+_{i+1/2} = \frac{1}{2}\ (k|a_{i+1/2}| - a_{i+1/2})$$

and

$$c^-_{i-1/2} = \frac{1}{2}\ (k|a_{i-1/2}| + a_{i-1/2})$$

Then $c^+_{i+1/2} \geqslant 0$, $c^-_{i-1/2} \geqslant 0$, provided that $k \geqslant 1$. In order to achieve a second order accurate scheme which satisfies the TVD condition, one need only apply the same sequence of operations defined by equations (5.3-5.6) to a corrected flux

$$F_i = f_i + g_i$$

in which g_i is an anti-diffusive flux which approximates

$$\Delta x \; \alpha \; \frac{\partial u}{\partial x} \quad ,$$

and thus cancels the first order error. It is necessary to limit the anti-diffusive flux, however, to prevent the possibility of $(g_{i+1} - g_i)/(u_{i+1} - u_i)$ becoming unbounded. For this purpose define

$$\tilde{g}_{i+1/2} = \alpha_{i+1/2}(u_{i+1} - u_i) \tag{5.7}$$

and

$$g_i = B(\tilde{g}_{i+1/2}, \tilde{g}_{i-1/2}) \tag{5.8}$$

where B is an averaging function which limits the magnitude attainable by $(g_{i+1} - g_i)/(u_{i+1} - u_i)$ and satisfies the condition

$$B(r,r) = r$$

A simple choice is the min mod function

$$B(r,s) = \begin{cases} 0 \text{ if } r \text{ and } s \text{ have opposite signs} \\ r \text{ if } |r| \leq |s| \text{ and } r \text{ and } s \text{ have the same sign} \\ s \text{ if } |s| \leq |r| \text{ and } r \text{ and } s \text{ have the same sign} \end{cases} \tag{5.9}$$

The numerical flux is now

$$h_{i+1/2} = \frac{1}{2}(f_{i+1} + f_i) + \frac{1}{2}(g_{i+1} + g_i) \tag{5.10}$$

$$-\alpha_{i+1/2}(u_{i+1} - u_i) - \frac{1}{2} k |g_{i+1} - g_i| \; \text{sign}(u_{i+1} - u_i)$$

In most of the domain the second term cancels the third term to order Δx^2, and the last term is of order Δx^2, yielding the desired second order accuracy.

Alternative flux limiting functions have been studied by Roe [21], and Sweby [22]. Let r_i be the ratio of consecutive gradients

$$r_i = \frac{\tilde{g}_{i-1/2}}{\tilde{g}_{i+1/2}} \quad .$$

One can set

$$B(\tilde{g}_{i+1/2}, \tilde{g}_{i-1/2}) = \phi(r_i)\tilde{g}_{i+1/2}$$

where the function ϕ satisfies the symmetry condition

$$\phi(r) = r\,\phi(1/r)$$

and

$$\phi(1) = 1$$

Then denoting $\phi(r_i)$ by ϕ_i,

$$\frac{g_{i+1} - g_i}{u_{i+1} - u_i} = \left(\frac{\phi_{i+1}}{r_{i+1}} - \phi_i\right) \alpha_{i+1/2}$$

which is bounded if $\phi(r)/r$ and $\phi(r)$ are bounded for all r. The resulting flux is

$$h_{i+1/2} = f_i + g_i - (\alpha_{i+1/2} - \frac{1}{2}\, a_{i+1/2})(u_{i+1} - u_i)$$

$$- 1/2 \left\{k \left| \frac{\phi_{i+1}}{r_{i+1}} - \phi_i \right| - \left(\frac{\phi_{i+1}}{r_{i+1}} - \phi_i\right)\right\}(u_{i+1} - u_i)$$

and it can be seen that the TVD condition (5.2) is satisfied.

The min mod function (5.9) is obtained by setting

$$\phi(r) = \begin{cases} 0, & r \leq 0 \\ r, & 0 \leq r \leq 1 \\ 1, & r \geq 1 \end{cases}$$

A less stringent limiter which may be expected to improve the accuracy is

$$\phi(r) = \frac{|r| + r}{1 + r}$$

Roe [21], Sweby [22], and Osher and Chakravarthy [6] have constructed TVD schemes which omit the last term of equation (5.10) by suitably restricting $\phi(r)$.

The concept of converting a first order monotone scheme to a second order scheme by adding an anti-diffusive flux which is limited to prevent spurious oscillations may already be found in the work of Boris, Book and Zalesak [13,14]. Harten's advance was to develop a mathematical formulation of the idea which allowed the TVD property to be proved for a second order scheme. The concept of flux limiting was independently introduced by van Leer [23].

There are difficulties in extending these ideas to systems of equations, and also to equations in more than one space dimension. Firstly the total variation of the solution of a system of hyperbolic equations may increase. Secondly it has been shown by Goodman and Leveque that a TVD scheme in two space dimensions is no better than first order accurate [24]. One might add dissipative terms by applying the same construction to the complete system of equations, using for $\alpha_{i+1/2}$ the spectral radius of the Jacobian matrix $\partial f/\partial u$, evaluated for an average value $u_{i+1/2}$. My own numerical experiments indicate that this leads to an excessively dissipative scheme. It can be seen however, that

with the scaling (4.4), the adaptive dissipation proposed in the previous section leads to a scheme which will behave locally like a TVD scheme if the constants are chosen to make sure that the coefficient $\varepsilon^{(2)}_{i+1/2,j} = 1/2$ in the neighborhood of a shock wave. This will be illustrated in Section 10 for the case of Burger's equation.

The discrimination needed for sharp resolution of shock waves in a fluid flow can be obtained by first decomposing the fluctuations into characteristic fields, following the suggestion set forth by Roe in a very striking paper [7]. The TVD construction is then separately applied to each field. For this purpose each flux difference is expressed in terms of components in the basis defined by the eigenvectors of $\partial f/\partial u$, evaluated at the interface. The dissipative terms are then defined separately for each field by equations (5.5)-(5.11), taking for $a_{i+1/2}$ the eigenvalues q, q, q+c and q-c of the different fields. The dissipative terms are finally recombined to form dissipative fluxes corresponding to the original variables.

Roe recommends that $\frac{\partial f}{\partial u}\Big|_{i+1/2}$ be represented by a matrix $A(u_{i+1},u_i)$ with the property that

$$A(u_{i+1},u_i)(u_{i+1} - u_i) = f_{i+1} - f_i$$

and has proposed a method of constructing such a matrix [8]. This has the advantage that a stationary shock wave can be resolved with a single interior point. Otherwise a non-oscillatory scheme will produce a smeared out shock wave with an extended tail.

These properties are not obtained without a cost. Firstly there is a large increase in the number of arithmetic operations required in the realization of the scheme. Secondly it is no longer possible to satisfy the design principle (4), stated in Section 1, that the total enthalpy of the steady state solution should be constant. Because the dissipative terms entering the mass and energy equations are independently constructed, these two equations are not consistent with each other in the steady state when the total enthalpy is constant.

There remains the pitfall of perhaps generating an unphysical solution which violates the entropy condition. The scheme defined by equations (5.3)-(5.10) allows a stationary discontinuous expansion. The flux is conserved across a stationary discontinuity of a solution of (5.1). Thus if u_{i+1} and u_i lie on either side of a stationary discontinuity, $f_{i+1} = f_i$, and according to equation (5.6) $a_{i+1/2} = 0$, with the result that the dissipative coefficient $\alpha_{i+1/2}$ defined by equation (5.5) also vanishes, and the difference equations are satisfied whether or not the discontinuity is an expansion or a compression. This difficulty can be corrected by modifying the definition of $\alpha_{i+1/2}$ to make sure that it cannot vanish in this situation.

6. Boundary Conditions

At a solid boundary the only contribution to the flux balance (3.3) comes from the pressure. The normal pressure gradient $\frac{\partial p}{\partial n}$ at the wall can be estimated from the condition that $\frac{\partial}{\partial t}(\rho q_n) = 0$, where q_n is the normal velocity component. The pressure at the wall is then estimated by extrapolation from the pressure at the adjacent cell centers, using the known value of $\frac{\partial p}{\partial n}$.

The rate of convergence to a steady state will be impaired if outgoing waves are reflected back into the flow from the outer boundaries. The treatment of the far field boundary condition is based on the introduction of Riemann invariants for a one dimensional flow normal to the boundary. Let subscripts ∞ and e denote free stream values and values extrapolated from the interior cells adjacent to the boundary, and let q_n and c be the velocity component normal to the boundary and the speed of sound. Assuming that the flow is subsonic at infinity, we introduce fixed and extrapolated Riemann invariants

$$R_\infty = q_{n\infty} - \frac{2c_\infty}{\gamma-1}$$

and

$$R_e = q_{n_e} + \frac{2c_e}{\gamma-1}$$

corresponding to incoming and outgoing waves. These may be added and subtracted to give

$$q_n = \frac{1}{2}(R_e + R_\infty)$$

and

$$c = \frac{\gamma-1}{4}(R_e - R_\infty)$$

where q_n and c are the actual normal velocity component and speed of sound to be specified in the far field. At an outflow boundary, the tangential velocity

component and entropy are extrapolated from the interior, while at an inflow boundary they are specified as having free stream values. These four quantities provide a complete definition of the flow in the far field. If the flow is supersonic in the far field, all the flow quantities are specified at an inflow boundary, and they are all extrapolated from the interior at an outflow boundary.

7. Hybrid Multistage Time Stepping Schemes

Multi-stage schemes for the numerical solution of ordinary differential equations are usually designed to give a high order of accuracy. Since the present objective is simply to obtain a steady state as rapidly as possible, the order of accuracy is not important. This allows the use of schemes selected purely for their properties of stability and damping. For this purpose it pays to distinguish the hyperbolic and parabolic parts stemming respectively from the convective and dissipative terms, and to treat them differently. This leads to a new class of hybrid multi-stage schemes.

Since the cell area S_{ij} is independent of time, equation (4.1) can be written as

$$\frac{dw}{dt} + R(w) = 0 \tag{7.1}$$

where R(w) is the residual

$$R_{i,j} = \frac{1}{S_{i,j}} (Q_{i,j} - D_{i,j}) \tag{7.2}$$

Let w^n be the value of w after n time steps. Dropping the subscripts i,j the general m stage hybrid scheme to advance a time step Δt can be written as

$$\begin{aligned}
w^{(0)} &= w^n \\
w^{(1)} &= w^{(0)} - \alpha_1 \Delta t R^{(0)} \\
&\cdots \\
w^{(m-1)} &= w^{(0)} - \alpha_{m-1} \Delta t R^{(m-2)} \\
w^{(m)} &= w^{(0)} - \Delta t R^{(m-1)} \\
w^{n+1} &= w^{(m)}
\end{aligned} \tag{7.3}$$

where the residual in the q+1st stage is evaluated as

$$R^{(q)} = \frac{1}{S} \sum_{r=0}^{q} \{\beta_{qr} Q(w^{(r)}) - \gamma_{qr} D(w^{(r)})\} \tag{7.4}$$

subject to the consistency constraint that

$$\sum_{r=0}^{q} \beta_{qr} = \sum_{r=0}^{q} \gamma_{qr} = 1 \tag{7.5}$$

In order to assess the properties of these schemes it is useful to consider the model problem

$$u_t + u_x + \mu \Delta x^3 u_{xxxx} = 0 \tag{7.6}$$

In the absence of the third order dissipative term this equation describes the propagation of a disturbance without distortion at unit speed. With centered differences the residual has the form

$$\Delta t R_i = \frac{\lambda}{2} (u_{i+1} - u_{i-1}) + \lambda\mu(u_{i+2} - 4u_{i+1} + 6u_i - 4u_{i-1} + u_{i-2})$$

where $\lambda = \Delta t/\Delta x$ is the Courant number. If we consider a Fourier mode $\hat{u} = e^{ipx}$ the discretization in space yields

$$\Delta t \frac{d\hat{u}}{dt} = z\hat{u}$$

where z is the Fourier symbol of the residual. Setting $\xi = p\Delta x$, this is

$$z = -\lambda i \sin\xi - 4\lambda\mu(1 - \cos\xi)^2 \tag{7.7}$$

A single step of the multistage scheme yields

$$\hat{u}^{n+1} = g(z)\hat{u}^{n}$$

where $g(z)$ is the amplification factor. The stability region of the scheme is given by those values of z for which $g(z) \leq 1$.

A simple procedure is to recalculate the residual at each stage using the most recently updated value of w. Then (7.4) becomes

$$R^{(q)} = \frac{1}{S}\left\{Q(w^{(q)}) - D(w^{(q)})\right\} \tag{7.8}$$

Schemes of this subclass have been analyzed in a book by van der Houwen [25], and more recently in papers by Sonneveld and van Leer [26], and Roe and Pike [27]. They are second order accurate in time for both linear and nonlinear problems if $\alpha_{m-1} = 1/2$. An efficient 4 stage scheme, which is also fourth order accurate for linear problems, has the coefficients

$$\alpha_1 = 1/4 \quad , \alpha_2 = 1/3 \quad , \alpha_3 = 1/2 \tag{7.9}$$

The amplification factor of this scheme is given by the polynomial

$$g\ (z) = 1 + z + \frac{z^2}{2} + \frac{z^3}{6} + \frac{z^4}{24}$$

The stability region of this scheme is shown in Figure 2(a), which displays contour lines for $|g| = 1, .9, .8, \ldots$. The Figure also shows the locus of z as the wave number is varied between 0 and 2π for a Courant number $\lambda = 2.8$, and a dissipation coefficient $\mu = 1/32$. The corresponding variation of $|g|$ with ξ is shown in Figure 2(b). The intercept of the stability region with the imaginary

axis is $2\sqrt{2}$; the corresponding bound on the time step is $\Delta t \leq 2\sqrt{2}\ \Delta x$.

The maximum stability interval along the imaginary axis attainable by an m stage scheme is m-1. This has been proved for the case when m is odd by van der Houwen, who also gave formulas for the coefficients α_q [25]. The case of m even has recently been solved by Sonneveld and van Leer [26]. For example, the 4 stage scheme with coefficients

$$\alpha_1 = 1/3,\ \alpha_2 = 4/15,\ \alpha_3 = 5/9$$

has a stability region extending to 3 along the imaginary axis, at the expense of a slight reduction along the real axis.

A substantial saving in computational effort can be realized by evaluating the dissipative part only once. This leads to a class of schemes in which (7.4) becomes

$$R^{(q)} = \frac{1}{S}\left\{Q(w^{(q)}) - D(w^{(0)})\right\} \tag{7.10}$$

The amplification factor can no longer be represented as a polynomial, but it can easily be calculated recursively. The stability region for a 4 stage scheme of this class with the coefficients (7.9) is shown in Figure 3. This also shows that this scheme is stable for the model problem (7.6) with a Courant number $\lambda = 2.6$, and dissipation coefficient $\mu = 1/32$. Schemes in the subclass defined by (7.10) are clearly more efficient than the more conventional schemes defined by (7.8), in which the dissipative terms are repeatedly evaluated.

If the time stepping scheme is to be used in a multigrid procedure it is important that it should be effective at damping high frequency modes. One can

fairly easily devise 3 and 4 stage schemes in the class defined by (7.10) which meet this requirement. An effective 3 stage scheme is given by the coefficients

$$\alpha_1 = .6, \qquad \alpha_2 = .6 \quad . \tag{7.11}$$

Its stability region is shown in Figure 4.

Additional flexibility is provided by a class of schemes in which the dissipative terms are evaluated twice. This may be used to make a further improvement in the high frequency damping properties, or else to extend the stability region along the real axis to allow more margin for the dissipation introduced by an upwind or TVD scheme of the type described in Section 5. In this class of schemes

$$\begin{aligned} R^{(0)} &= \frac{1}{S}\left\{Qw^{(0)}) - Dw^{(0)})\right\} \\ R^{(q)} &= \frac{1}{S}\left\{Q(w^{(q)}) - \beta D(w^{(1)}) - (1-\beta)D(w^{(0)})\right\}, \quad q \geqslant 1 \end{aligned} \tag{7.12}$$

In the case of pure dissipation (Qw = 0), the amplification factor reduces to

$$g = 1 + z + \alpha_1\beta\, z^2$$

Thus if β is chosen such that $\alpha_1\beta = 1/4$, the stability region will contain a double zero at $z = -2$ on the real axis. A maximum stability interval of 8 can be attained along the real axis by choosing β such that $\alpha_1\beta = 1/8$. Figures 5 and 6 show stability regions of 4 and 5 stage schemes in this class with the coefficients

$$\alpha_1 = 1/4, \quad \alpha_2 = 1/3, \quad \alpha_3 = 1/2, \quad \beta = 1 \qquad (7.13)$$

and

$$\alpha_1 = 1/4, \quad \alpha_2 = 1/6, \quad \alpha_3 = 3/8, \quad \alpha_4 = 1/2, \quad \beta = 1 \qquad (7.14)$$

The improvement of Figure 5 over Figure 2 is clear. The 5 stage scheme combines van der Houwen's optimal coefficients with two evaluations of the dissipative terms to attain a stability interval of 4 along both the imaginary and the real axes.

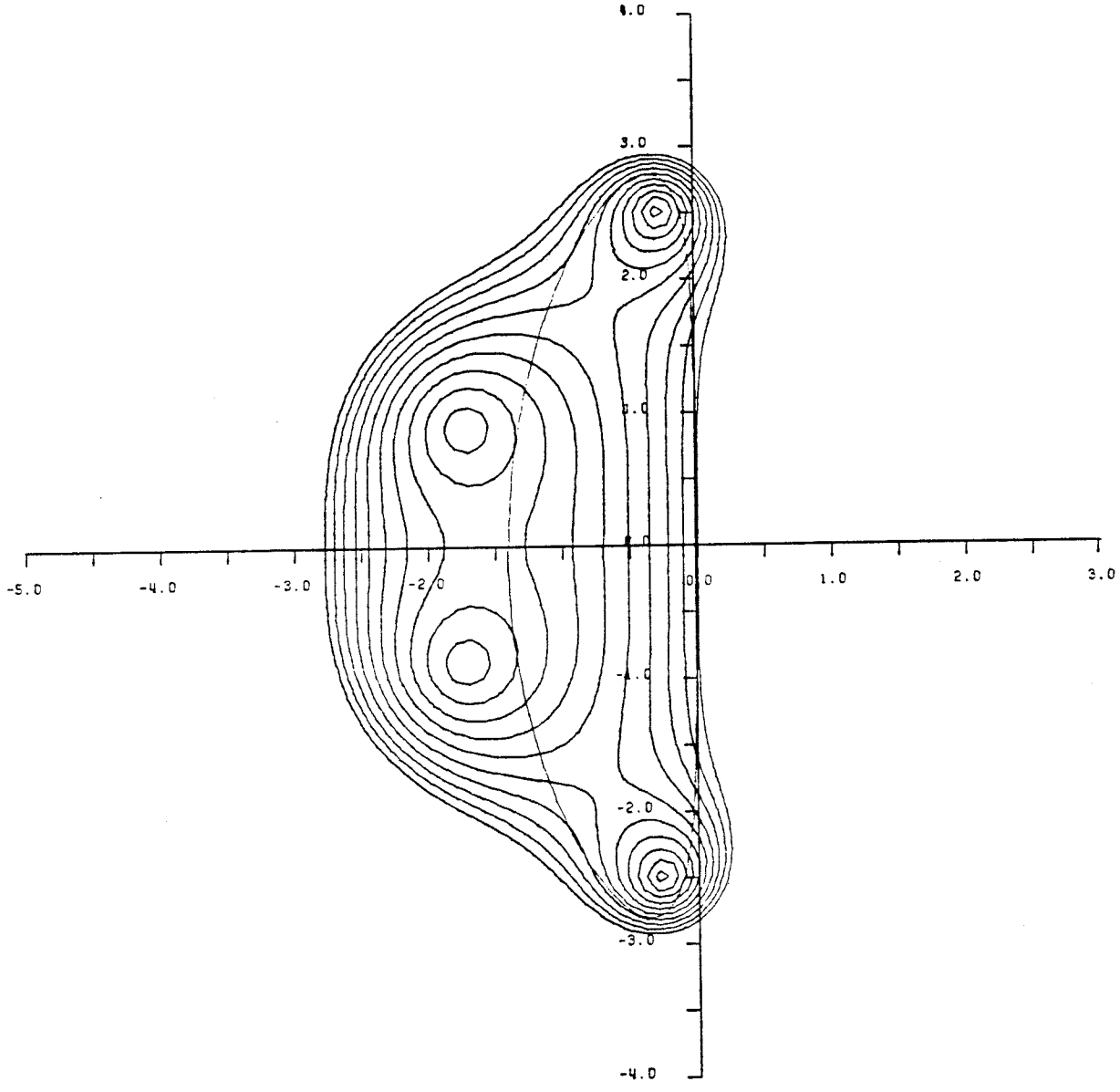

Figure 2(a)

Stability region of standard 4 stage scheme
Contour lines $|g| = 1., .9, .8, \ldots$
and locus of $z(\xi)$ for $\lambda = 2.8$, $\mu = 1/32$
Coefficients $\alpha_1 = 1/4$, $\alpha_2 = 1/3$, $\alpha_3 = 1/2$

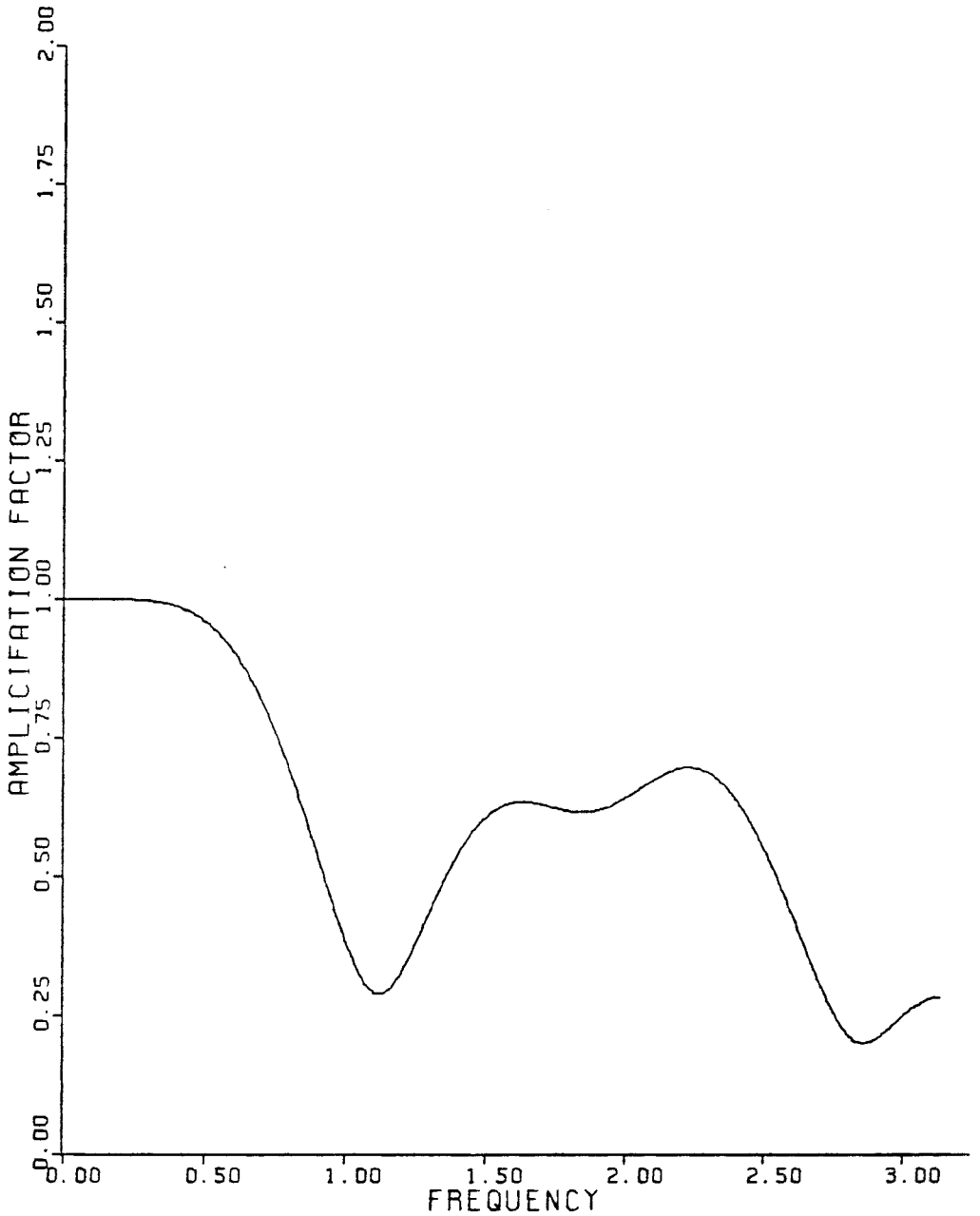

Figure 2(b)

Amplification factor $|g|$ of standard 4 stage scheme
for $\lambda = 2.8$, $\mu = 1/32$
Coefficients $\alpha_1 = 1/4$, $\alpha_2 = 1/3$, $\alpha_3 = 1/2$

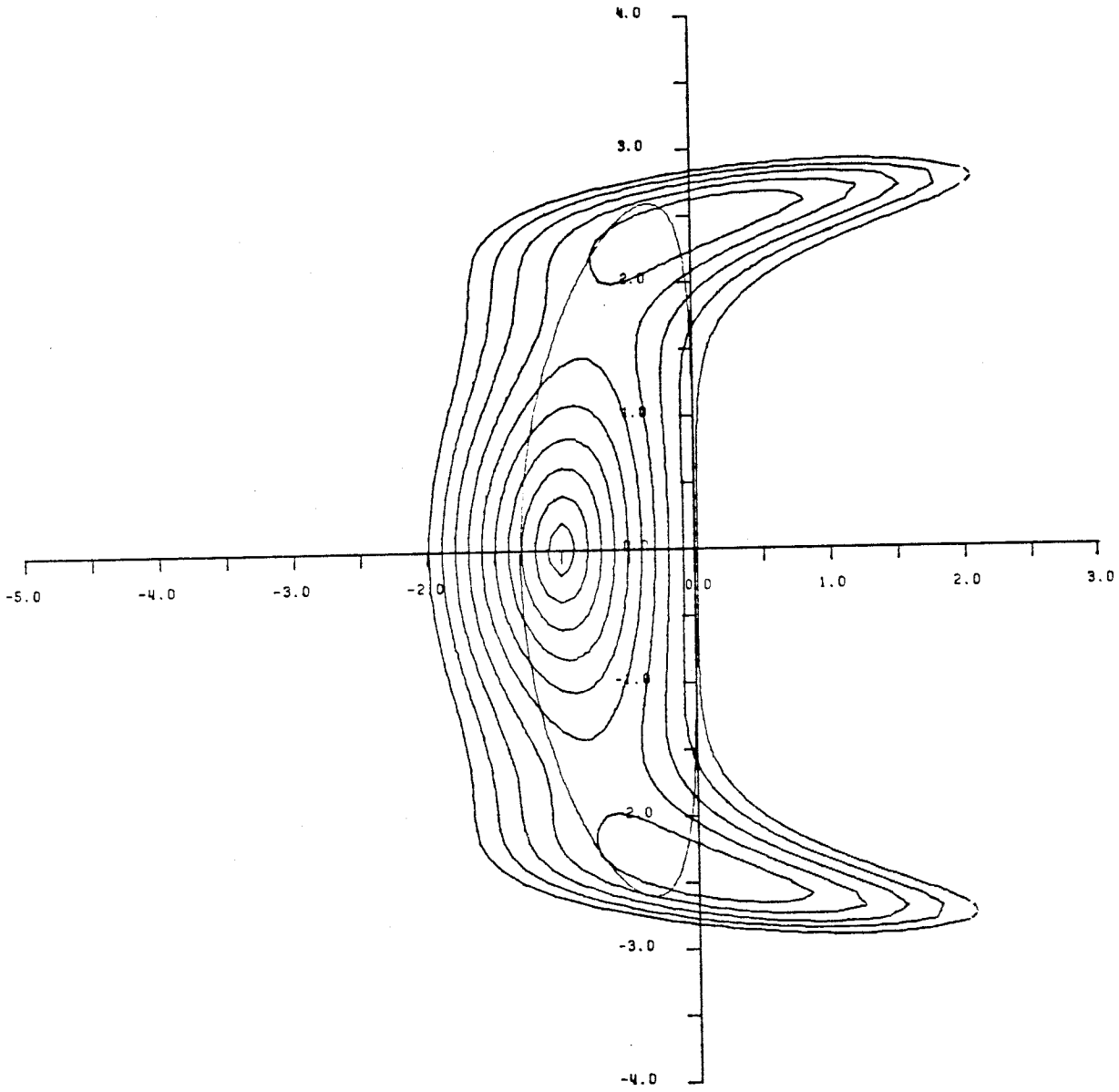

Figure 3(a)

Stability region of 4 stage scheme with single evaluation of dissipation
Contour lines $|g|$ = 1., .9, .8, ...
and locus of $z(\xi)$ for λ = 2.6, μ = 1/32
Coefficients α_1 = 1/4, α_2 = 1/3, α_3 = 1/2

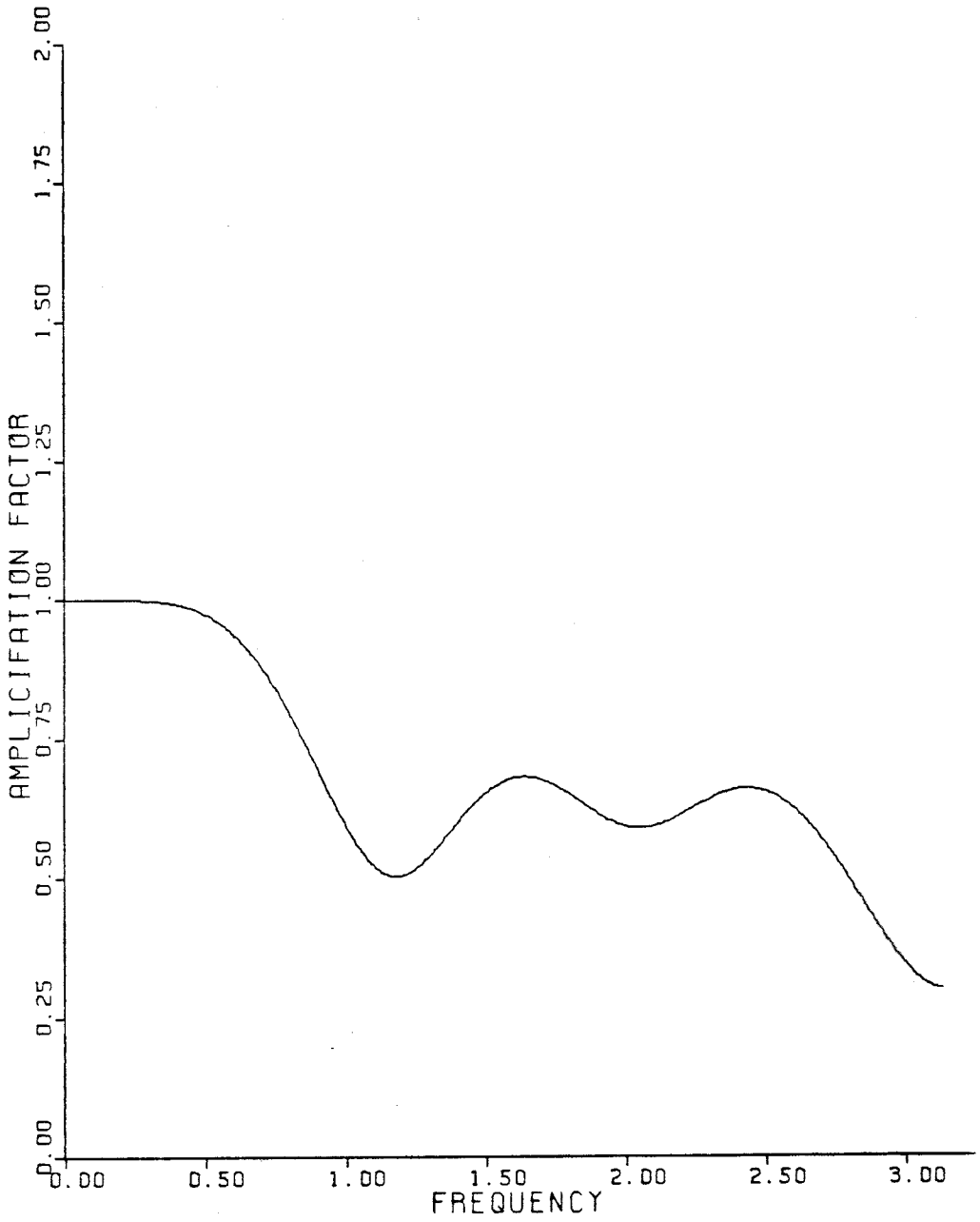

Figure 3(b)

Amplification factor $|g|$ of 4 stage scheme with single evaluation of dissipation for $\lambda = 2.6$, $\mu = 1/32$
Coefficients $\alpha_1 = 1/4$, $\alpha_2 = 1/3$, $\alpha_3 = 1/2$

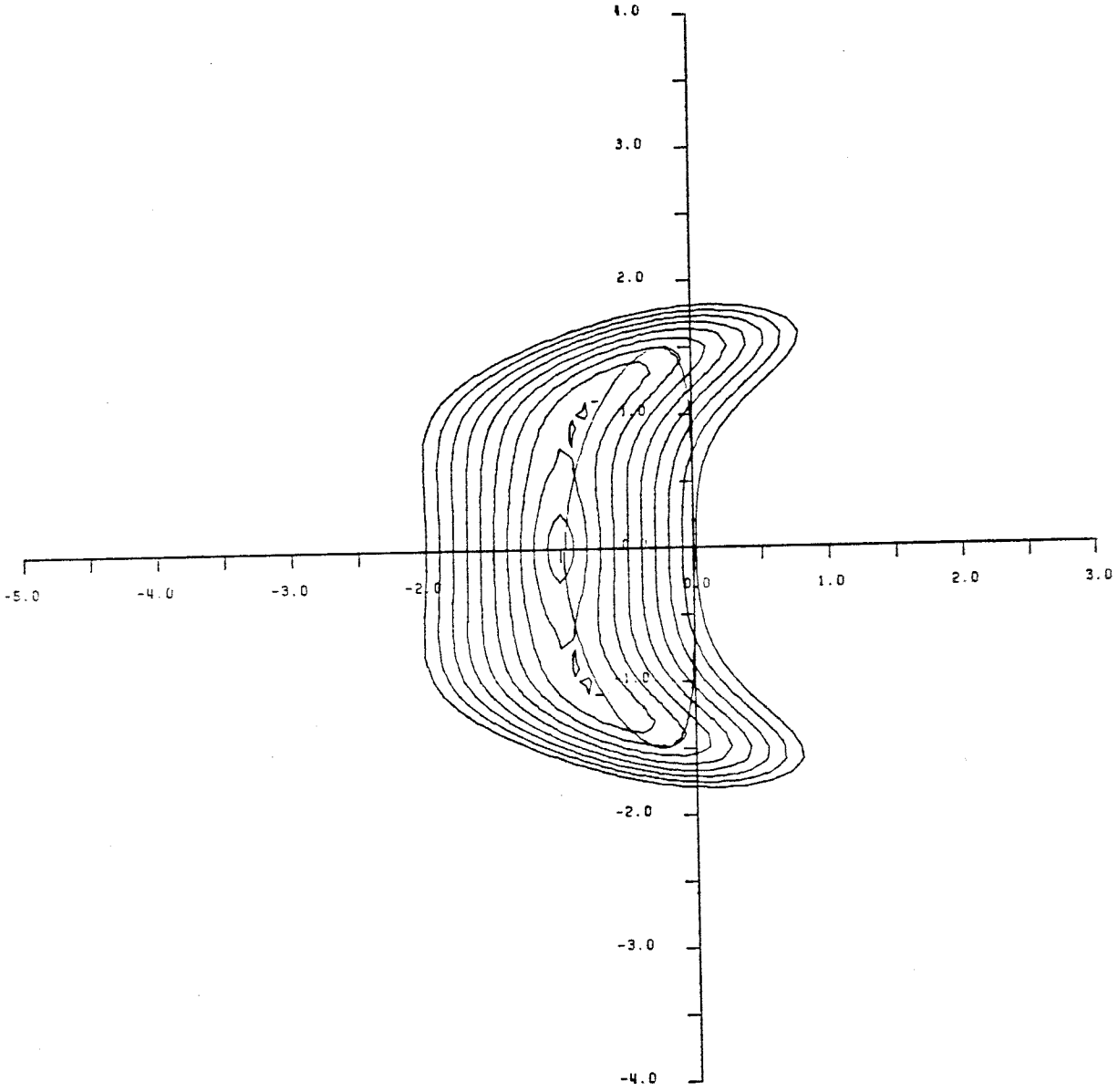

Figure 4(a)

Stability region of 3 stage scheme with single evaluation of dissipation
Contour lines $|g| = 1., .9, .8, \ldots$
and locus of $z(\xi)$ for $\lambda = 1.5$, $\mu = .04$
Coefficients $\alpha_1 = .6$, $\alpha_2 = .6$

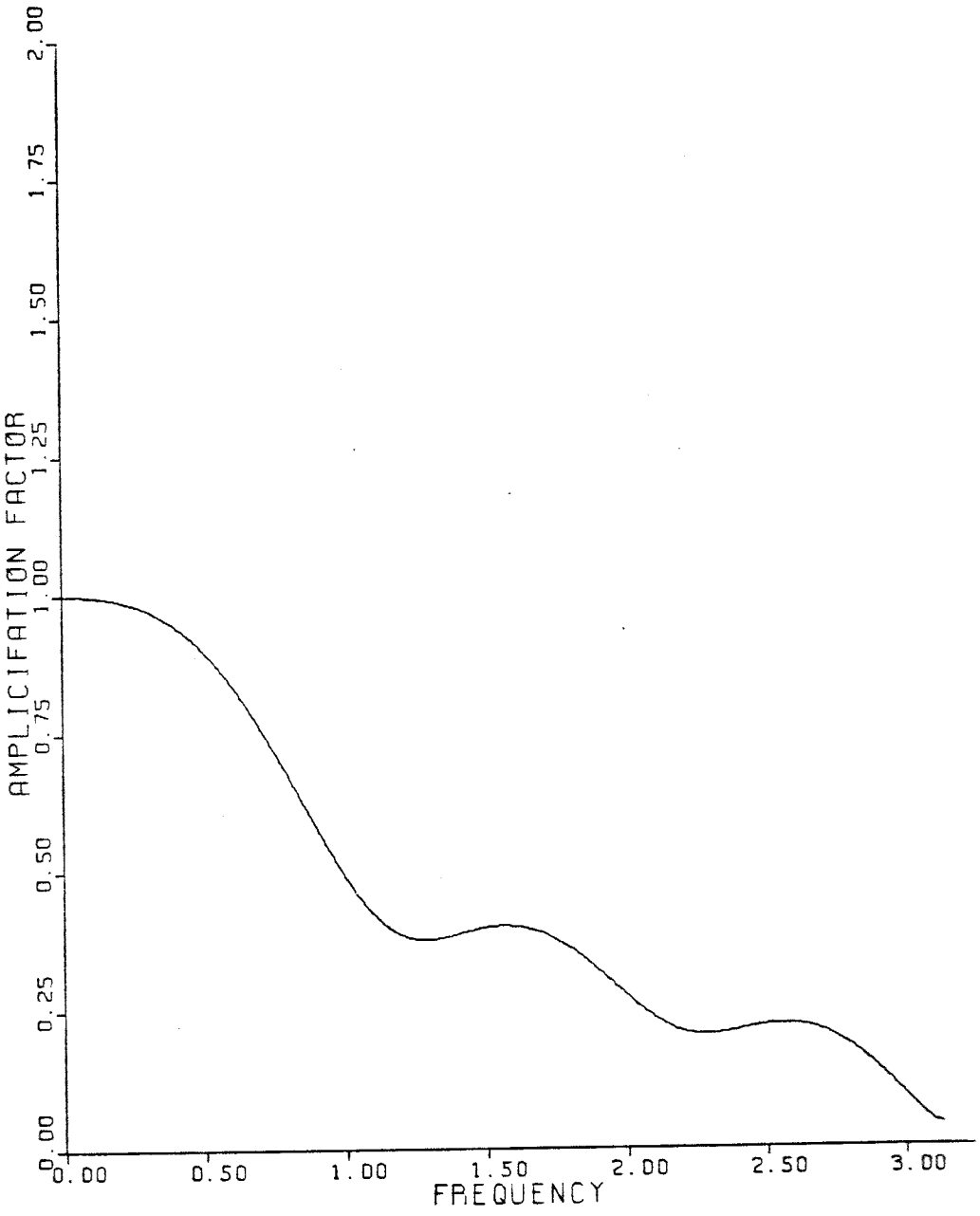

Figure 4(b)

Amplification factor $|g|$ of 3 stage scheme with
single evaluation of dissipation
for $\lambda = 1.5$, $\mu = .04$
Coefficients $\alpha_1 = .6$, $\alpha_2 = .6$

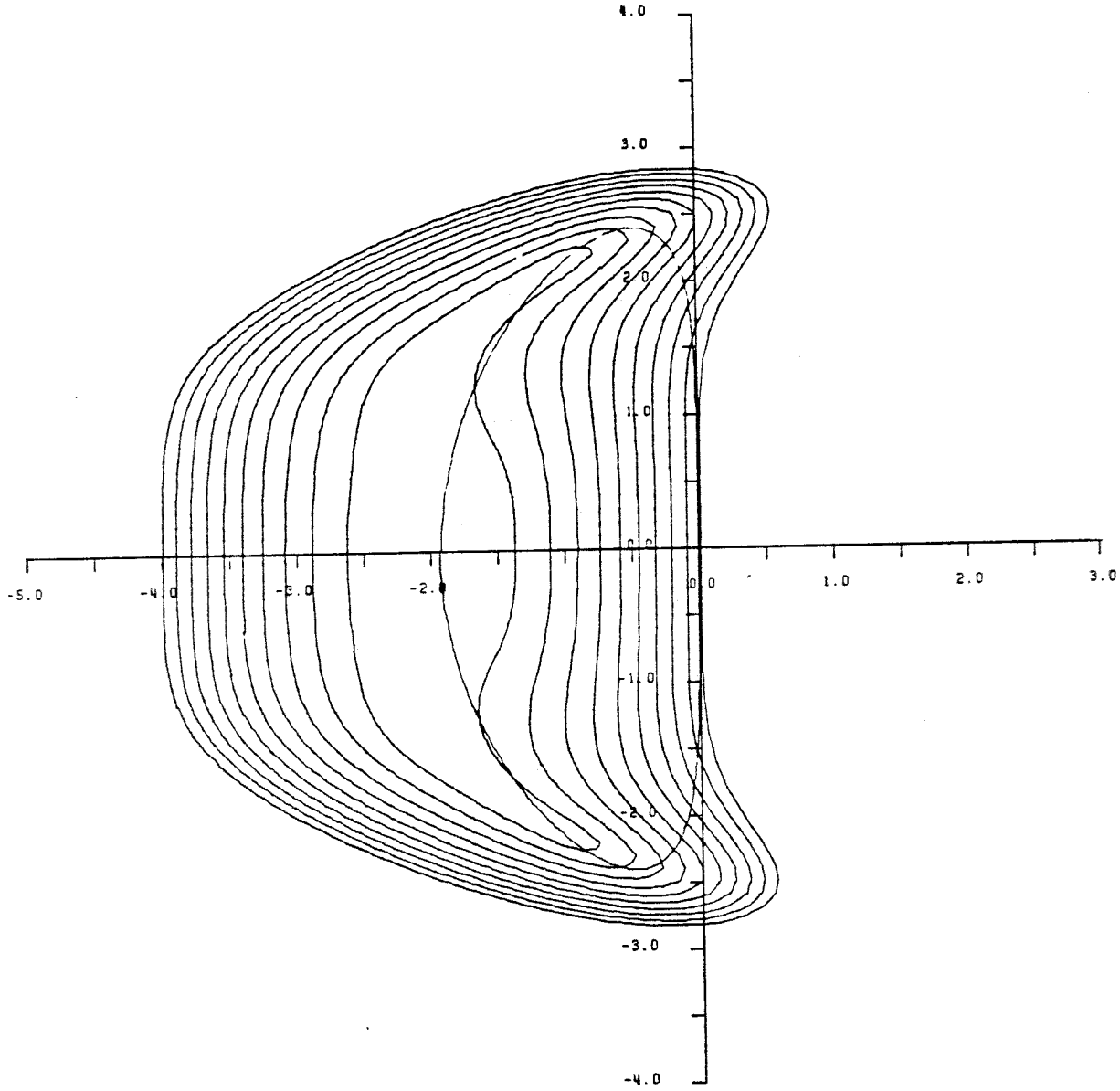

Figure 5(a)

Stability region of 4 stage scheme with two evaluations of dissipation
Contour lines $|g|$ = 1., .9, .8, ...
and locus of $z(\xi)$ for $\lambda = 2.4$, $\mu = .05$
Coefficients $\alpha_1 = 1/4$, $\alpha_2 = 1/3$, $\alpha_3 = 1/2$, $\beta = 1$

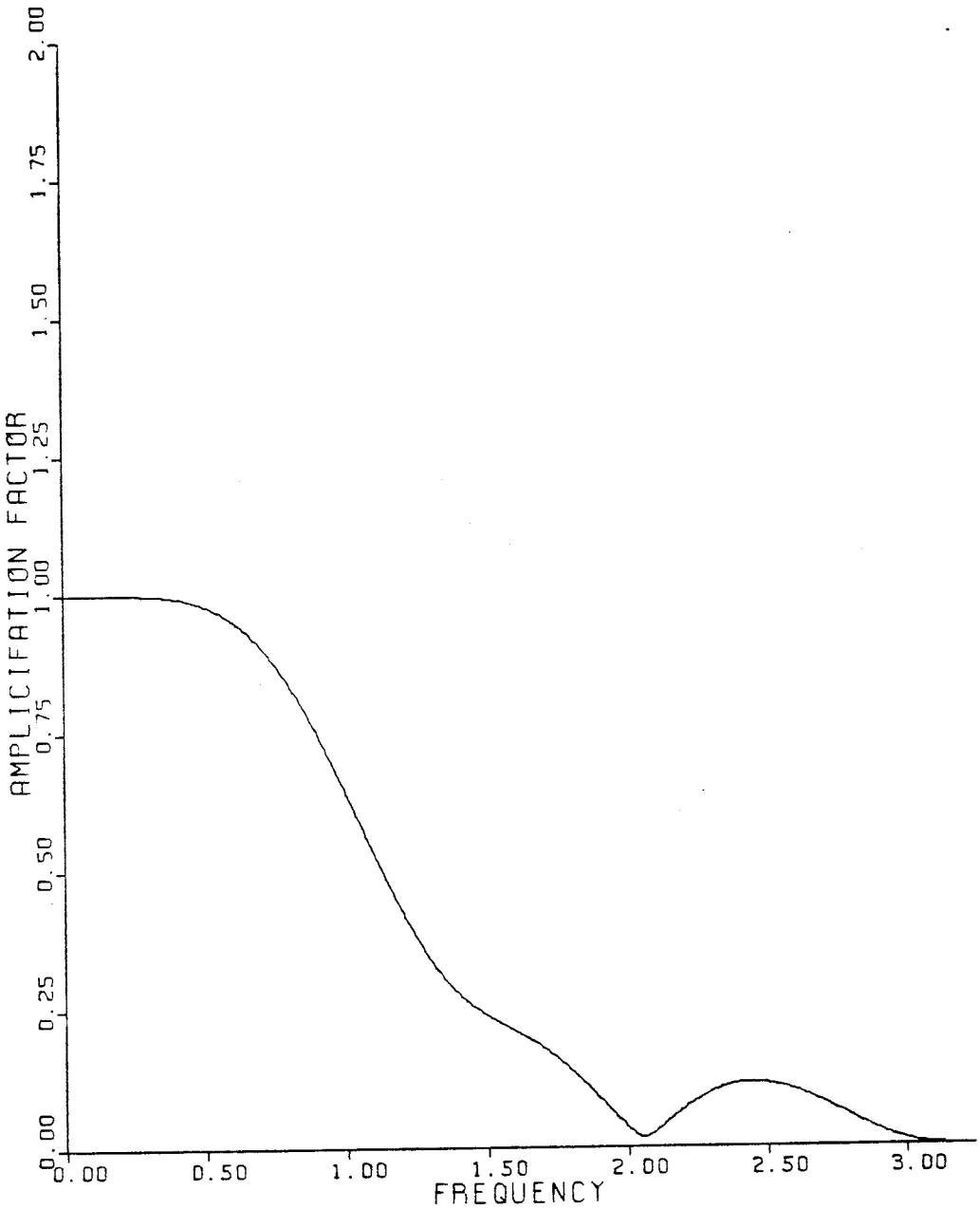

Figure 5(b)

Amplification factor 4 stage scheme
with two evaluations of dissipation
for $\lambda = 2.4$, $\mu = .05$
Coefficients $\alpha_1 = 1/4$, $\alpha_2 = 1/3$, $\alpha_3 = 1/2$, $\beta = 1$

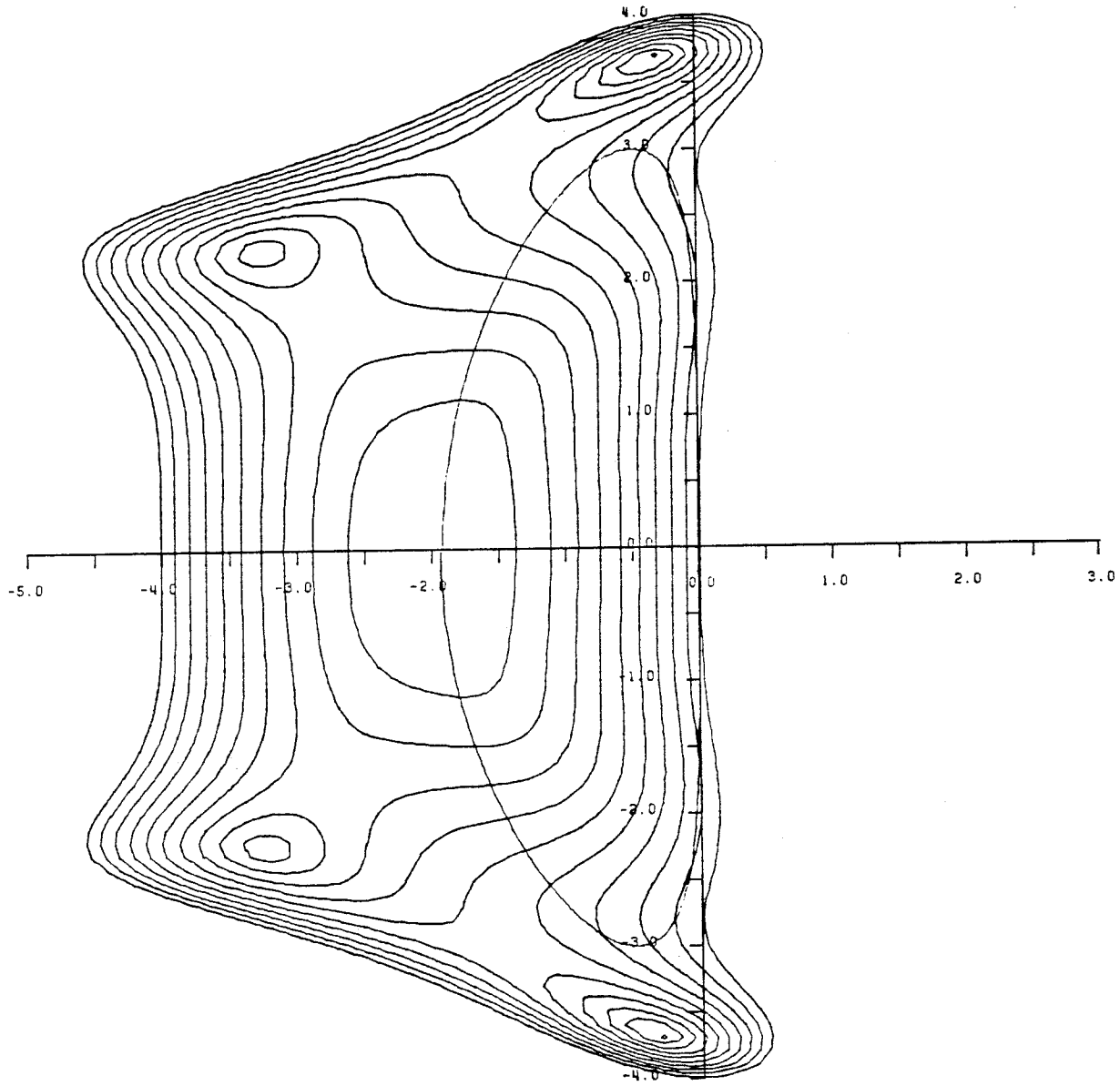

Figure 6(b)

Amplification factor $|g|$ of 5 stage scheme with
with two evaluations of dissipation
for $\lambda = 3$, $\mu = .04$
Coefficients $\alpha_1 = 1/4$, $\alpha_2' = 1/6$, $\alpha_3 = 3/8$, $\alpha_4 = 1/2$, $\beta = 1$

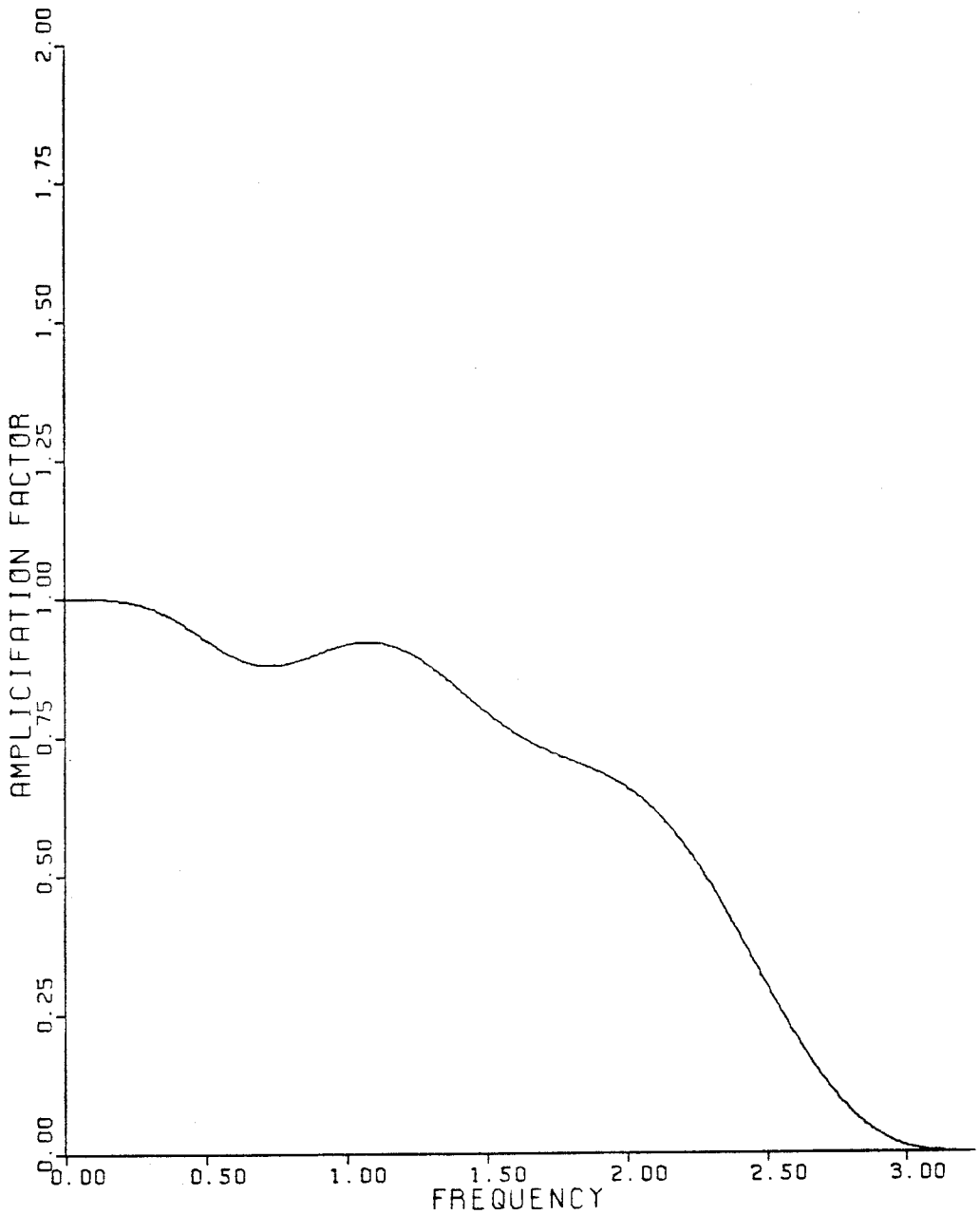

Figure 6(a)

Stability region of 5 stage scheme with two evaluations of dissipation
Contour lines $|g| = .9, .8, .7, \ldots$
and locus of $z(\xi)$ for $\lambda = 3.$, $\mu = .04$
Coefficients $\alpha_1 = 1/4$, $\alpha_2 = 1/6$, $\alpha_3 = 3/8$, $\alpha_4 = 1/2$, $\beta = 1$

8. Residual Averaging

A simple method of increasing the time step is to replace the residuals by weighted averages of the neighboring residuals [28]. Consider the general multi-stage scheme (7.3). In a one dimensional case one might replace the residual R_i by the average

$$\bar{R}_i = \varepsilon R_{i-1} + (1-2\varepsilon) R_i + \varepsilon R_{i+1} \tag{8.1}$$

at each stage of the scheme. This smooths the residuals and also increases the support of the scheme, thus relaxing the restriction on the time step imposed by the Courant-Friedrichs-Lewy condition. If $\varepsilon \geq 1/4$, however, there are Fourier modes such that $\bar{R}_i = 0$ when $R_i \neq 0$. To avoid this restriction one may perform the averaging implicitly by setting

$$-\varepsilon \bar{R}_{i-1} + (1+2\varepsilon)\bar{R}_i - \varepsilon \bar{R}_{i+1} = R_i \tag{8.2}$$

For an infinite interval this equation has the explicit solution

$$R_i = \frac{1-r}{1+r} \sum_{q=-\infty}^{\infty} r^q R_{i+q} \tag{8.3}$$

where

$$\varepsilon = \frac{r}{(1-r)^2} \quad , \; r < 1 \tag{8.4}$$

Thus the effect of the implicit smoothing is to collect information from residuals at all points in the field, with an influence coefficient which decays by factor r at each additional mesh interval from the point of interest.

Consider the model problem (7.6). According to equation (8.4) the Fourier symbol (7.7) will be replaced by

$$z = -\lambda \frac{i \sin \xi + 4\mu(1-\cos\xi)^2}{1 + 2\varepsilon(1-\cos\xi)}$$

In the absence of dissipation one now finds that stability can be maintained for any Courant number λ, provided that the smoothing parameter satisfies

$$\varepsilon \geqslant \frac{1}{4}\left\{\frac{\lambda^2}{\lambda^{*2}} - 1\right\}$$

where λ^* is the stability limit of the unsmoothed scheme. In terms of the decay parameter r the stability condition becomes

$$\frac{1+r}{1-r} \geqslant \frac{\lambda}{\lambda^*}$$

Suppose that the time step is increased to the limiting value permitted by a given value of r. Then according to (8.3) the Fourier symbol in the absence of dissipation is

$$z = -\lambda^* \left\{1 + 2 \sum_{q=1}^{\infty} r^q \cos q\xi\right\} i\sin\xi$$

$$= -\lambda^* \frac{1-r^2}{1-2r\cos\xi+r^2} i\sin\xi$$

and it may be verified that $|z| \leqslant \lambda^*$.

In the case of a finite interval with periodic conditions equation (8.3) still holds, provided that the values R_{i+q} outside the interval are defined by periodicity. In the absence of periodicity one can also choose boundary conditions such that (8.3) is a solution of (8.2), with $R_{i+q} = 0$ if i + q lies out-

side the interval. This solution can be realized by setting

$$\tilde{R}_1 = R_1$$

$$\tilde{R}_i = R_i - r(R_i - \tilde{R}_{i-1}) \text{ for } 2 \leqslant i \leqslant n$$

and then

$$\bar{R}_n = \frac{1}{1 + r} \tilde{R}_n$$

$$\bar{R}_i = \tilde{R}_i - r(\tilde{R}_i - \bar{R}_{i+1}) \text{ for } 1 \leqslant i \leqslant n-1$$

In the two dimensional case the implicit residual averaging is applied in product form

$$(1-\varepsilon_x \delta_x^2)(1-\varepsilon_y \delta_y^2) \bar{R}_{ij} = R_{ij}$$

where δ_x^2 and δ_y^2 are the second difference operators in the x and y directions, and ε_x and ε_y are the corresponding smoothing parameters.

In practice the best rate of convergence is generally obtained by using a value of λ about three times λ^*, and the smallest possible amount of smoothing to maintain stability. The idea of residual averaging may be compared with Lerat's implicit scheme [29]. This may be interpreted as a method of smoothing the corrections calculated by a 2 stage scheme. In the general case of an m stage scheme it is not sufficient to smooth the final corrections after the mth stage, It is possible, however, to devise stable schemes by smoothing the residuals at alternate stages, starting with the 1st stage if m is odd, and the 2nd stage if m is even.

9. Multigrid Scheme

While the available theorems in the theory of multigrid methods generally assume ellipticity, it seems that it ought to be possible to accelerate the evolution of a hyperbolic system to a steady state by using large time steps on coarse grids, so that disturbances will be more rapidly expelled through the outer boundary. The interpolation of corrections back to the fine grid will introduce errors, however, which cannot be rapidly expelled from the fine grid, and ought to be locally damped if a fast rate of convergence is to be attained. Thus it remains important that the driving scheme should have the property of rapidly damping out high frequency modes.

In a novel multigrid scheme proposed by Ni [30], the flow variables are stored at mesh nodes, and the rates of change of mass, momentum and energy in each mesh cell are estimated from the flux integral appearing in equation (3.1). The corresponding change δw in the flow variables is then distributed unequally between the nodes at its four corners. The distribution rule is such that the accumulated corrections at each node correspond to the first two terms of a Taylor series in time, like a Lax Wendroff scheme. As it stands, this scheme does not damp oscillations between odd and even points. Ni introduces artificial viscosity by adding a further correction proportional to the difference between the value at each corner and the average of the values at the four corners of the cell. Residuals on the coarse grid are formed by taking weighted averages of the corrections at neighboring nodes of the fine grid, and corrections are then assigned to the corners of corase grid cells by the same distribution rule. When several grid levels are used, the distribution rule is applied once on each grid down to the coarsest grid, and the corrections are

then interpolated back to the fine grid. Using 3 or 4 grid levels, Ni obtained a mean rate of convergence of about .95, measured by the average reduction of the residuals in a multigrid cycle. The performance of the scheme seems to depend critically on the presence of the added dissipative terms to provide the necessary damping of high frequency nodes. In Ni's published version of the scheme these introduce an error of first order.

The flexibility in the formulation of the hybrid multi-stage schemes allows them to be designed to provide effective damping of high frequency modes with higher order dissipative terms. This makes it possible to devise rapidly convergent multigrid schemes without any need to compromise the accuracy through the introduction of excessive levels of dissipation [31].

In order to adapt the multi-stage scheme for a multigrid algorithm , auxiliary meshes are introduced by doubling the mesh spacing. Values of the flow variables are transferred to a coarser grid by the rule

$$w_{2h}^{(0)} = (\sum S_h w_h)/S_{2h} \tag{9.1}$$

where the subscripts denote values of the mesh spacing parameter, S is the cell area, and the sum is over the 4 cells on the fine grid composing each cell on the coarse grid. This rule conserves mass, momentum and energy. A forcing function is then defined as

$$P_{2h} = \sum R_h(w_h) - R_{2h}(w_{2h}^{(0)}) \tag{9.2}$$

where R is the residual of the difference scheme. In order to update the solution on a coarse grid, the multistage scheme (7.3) is reformulated as

$$
\begin{aligned}
w^{(1)} &= w_{2h}^{(0)} - \alpha_1 \Delta t (R_{2h}^{(0)} + P_{2h}) \\
&\cdots \\
w_{2h}^{(q+1)} &= w_{2h}^{(0)} - \alpha_q \Delta t \ (R_{2h}^{(q)} + P_{2h}) \\
&\cdots
\end{aligned}
\tag{9.3}
$$

where $R^{(q)}$ is the residual at the $q+1^{st}$ stage. In the first stage of the scheme, the addition of P_{2h} cancels $R_{2h}(w_{2h}^{(0)})$ and replaces it by $\sum R_h(w_h)$, with the result that the evolution on the coarse grid is driven by the residuals on the fine grid. This process is repeated on successively coarser grids. Finally the correction calculated on each grid is passed back to the next finer grid by bilinear interpolation.

Since the evolution on a coarse grid is driven by residuals collected from the next finer grid, the final solution on the fine grid is independent of the choice of boundary conditions on the coarse grids. The surface boundary condition is treated in the same way on every grid, by using the normal pressure gradient to extrapolate the surface pressure from the pressure in the cells adjacent to the wall. The far field conditions can either be transferred from the fine grid, or recalculated by the procedure described in Section 6.

It turns out than an effective multigrid strategy is to use a simple saw tooth cycle (as illustrated in Figure 7), in which a transfer is made from each grid to the next coarser grid after a single time step. After reaching the coarsest grid the corrections are then successively interpolated back from each grid to the next finer grid without any intermediate Euler calculations. On each grid the time step is varied locally to yield a fixed Courant number, and the same Courant number is generally used on all grids, so that progressively larger time steps are used after each transfer to a coarser grid. In comparison

with a single time step of the Euler scheme on the fine grid, the total computational effort in one multigrid cycle is

$$1 + 1/4 + 1/16 + \ldots \leq 4/3$$

plus the additional work of calculating the forcing functions P, and interpolating the corrections.

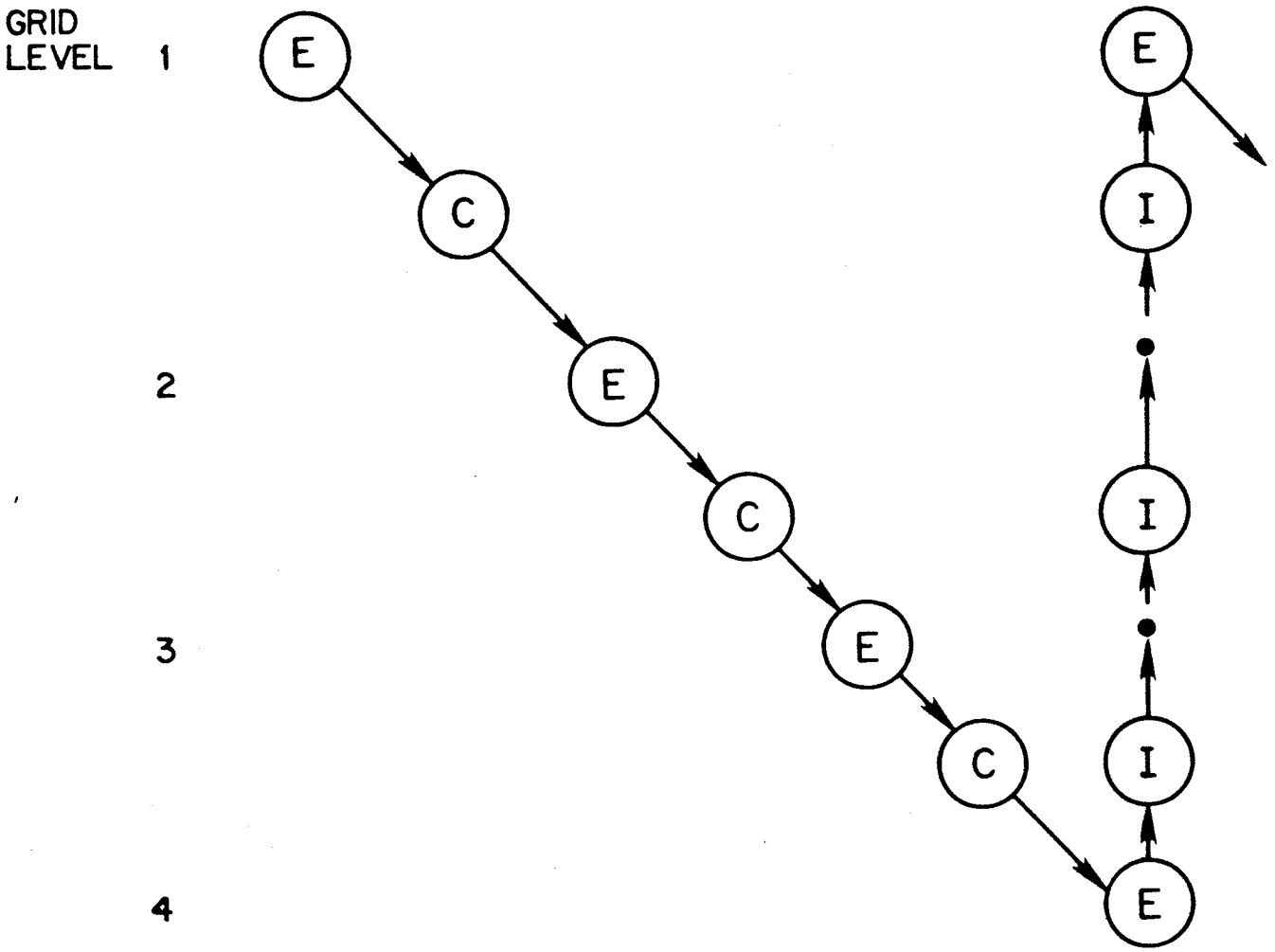

Figure 7

Saw Tooth Multigrid Cycle

(E) Euler Calculation

(C) Residual Collection

(I) Interpolation

10. Trials with Burger's Equation

The simplest nonlinear conservation law is Burger's equation without viscosity:

$$\frac{\partial u}{\partial t} + \frac{\partial}{\partial x}\left(\frac{u^2}{2}\right) = 0 \tag{10.1}$$

This provides a useful test of the properties of numerical schemes which avoids other complicating factors such as boundary conditions and complex geometry. If the boundary conditions are given as

$$u(0) = v, \qquad u(1) = -v, \qquad v \geq 0 \tag{10.2}$$

equation (10.1) admits a steady entropy satisfying solution with a shock wave at a location which depends on the initial state. This section presents the results of some numerical experiments in which the multigrid multi-stage time stepping scheme was applied to initial data satisfying (10.2), to test its ability to recover a steady solution. The semi-discretization has the form

$$\frac{du_i}{dt} + \frac{1}{\Delta x}\left(f_{i+1/2} - f_{i-1/2} - d_{i+1/2} + d_{i-1/2}\right) = 0$$

where $f_{i+1/2}$ is the convective flux

$$f_{i+1/2} = 1/4(u_{i+1}^2 + u_i^2)$$

and $d_{i+1/2}$ is the artificial dissipative flux.

Several alternative forms of the dissipative flux were tested:

1). Adaptive Dissipation (Section 4)

$$d_{i+1/2} = \varepsilon^{(2)}_{i+1/2}\ \alpha_{i+1/2}\ (u_{i+1} - u_i)$$

$$- \varepsilon^{(4)}_{i+1/2}\ \alpha_{i+1/2}\ (u_{i+2} - 3u_{i+1} + 3u_i - u_{i-1})$$

where

$$\alpha_{i+1/2} = \frac{1}{4} \left| u_{i+1} + u_i \right| \qquad \text{(scheme 1a)}$$

or

$$\alpha_{i+1/2} = \frac{1}{4} \left\{ \left| u_{i+1} \right| + \left| u_i \right| \right\} \qquad \text{(scheme 1b)}$$

Also $\varepsilon^{(2)}_{i+1/2}$ and $\varepsilon^{(4)}_{i+1/2}$ are determined by defining a sensor

$$\nu_i = 2 \frac{\left| u_{i+1} - 2u_i + u_{i-1} \right|}{\left| u_{i+1} \right| + 2 \left| u_i \right| + \left| u_{i-1} \right|}$$

Set

$$\bar{\nu}_{i+1/2} = \max (\nu_{i+2}, \nu_{i+1}, \nu_i, \nu_{i-1})$$

Then

$$\varepsilon^{(2)}_{i+1/2} = \min (k^{(2)}, \bar{\nu}_{i+1/2})$$

and

$$\varepsilon^{(4)}_{i+1/2} = \max (0, k^{(4)} - \bar{\nu}_{i+1/2})$$

By choosing $k^{(2)} = 1$ the scheme is locally TVD wherever $\nu_{i+1/2} \geq 1$.

2). TVD Scheme (Section 5)

$$d_{i+1/2} = \alpha_{i+1/2}(u_{i+1} - u_i) - \frac{1}{2}(g_{i+1} + g_i)$$

$$+ \frac{1}{2} |g_{i+1} - g_i| \text{sign}(u_{i+1} - u_i)$$

where

$$\alpha_{i+1/2} = \frac{1}{4} |u_{i+1} + u_i| \qquad \text{(scheme 2a)}$$

or

$$\alpha_{i+1/2} = \frac{1}{4} \{|u_{i+1}| + |u_i|\} \qquad \text{(scheme 2b)}$$

Also the anti-diffusive flux g_i is determined by

$$\tilde{g}_{i+1/2} = \alpha_{i+1/2}(u_{i+1} - u_i)$$

and

$$g_i = B(\tilde{g}_{i+1/2}, \tilde{g}_{i-1/2})$$

where B(r,s) is the min mod function (5.9). The choice of $\alpha_{i+1/2}$ in schemes 1a and 2a allows a stationary shock with at most one interior point, but also allows a stationary expansion shock. The alternative form used in schemes 1b and 2b excludes the stationary expansion shock, and still allows a discrete shock with no tail, but now with 2 interior points, as may be verified solving a quadratic equation.

Calculations were performed with a 3 stage time stepping scheme in which the dissipative terms were evaluated twice, as defined by equations (7.3) and (7.12), with the coefficients

$$\alpha_1 = .6 \quad , \alpha_2 = .6, \quad \beta = .35$$

The stability region of this scheme is shown in Figure 8. The grid contained 128 cells, and 5 grid levels were used in the multigrid scheme.

Figure 9 shows a typical evolution using scheme 1a. Figure 9(a) shows the first 10 time steps, starting from the initial data at the bottom of the figure. It can be seen that by the completion of the 6th step the solution is indistinguishable from the final steady solution, illustrated in Figure 9(b). In this case the symmetry of the initial data results in a shock wave with no interior points. The convergence history measured by the average value of $|\partial u/\partial t|$ is shown in Figure 9(c). Figure 10 shows a similar evolution with shifted initial data. The shock wave in the final steady state is displaced to the right and contains a single interior point, as a consequence of the choice of the viscosity coefficient $\alpha_{i+1/2}$. Figure 11 shows the first calculation repeated with scheme 1b. The final solution now has a shock wave with 2 interior points because of the additional dissipation introduced by the choice of an entropy satisfying viscosity coefficient. The TVD schemes 2a and 2b produced results which were essentially identical to those produced by schemes 1a and 1b, but with a slower rate of convergence to a steady state.

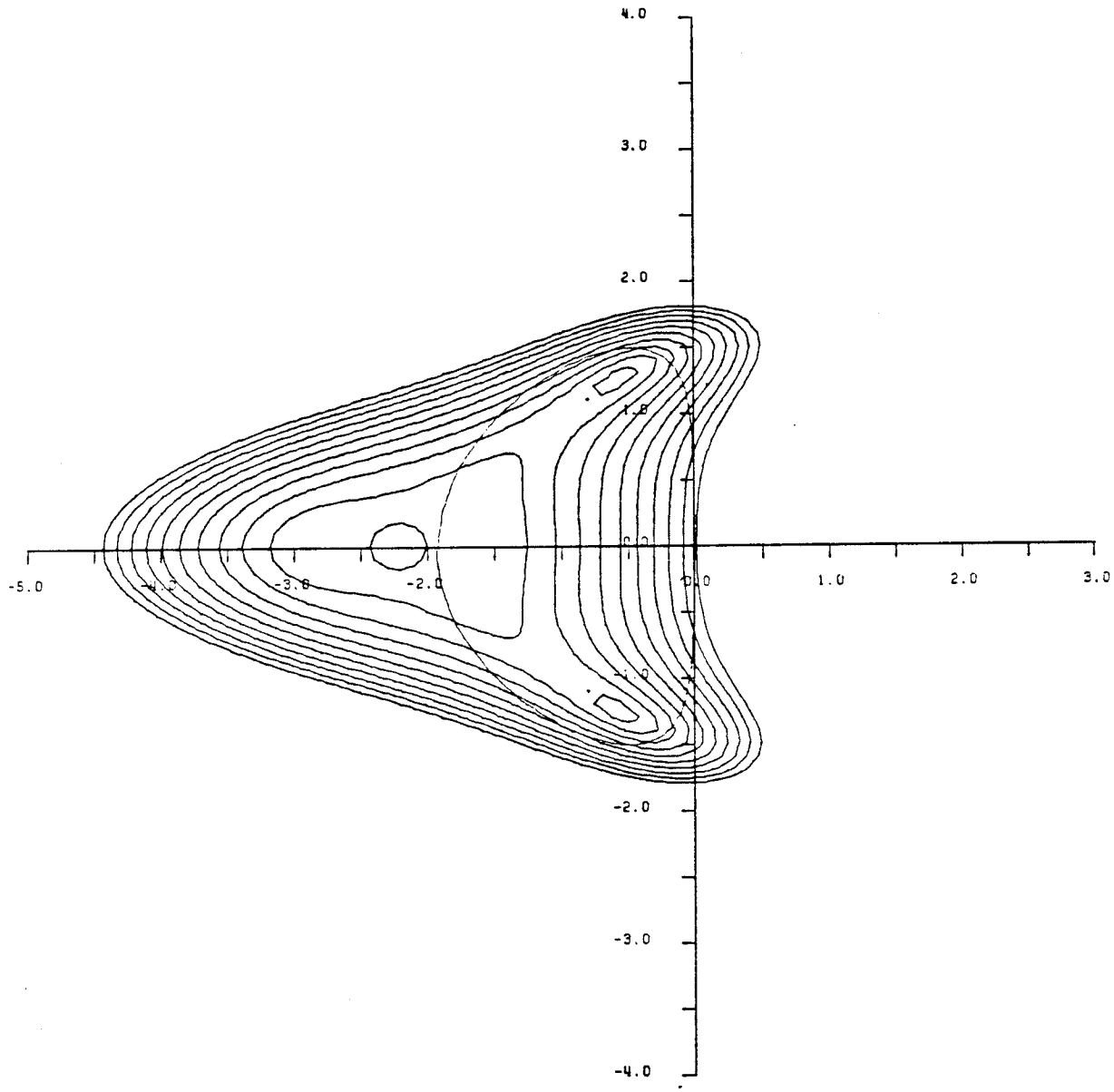

Figure 8

Stability region of 3 stage scheme with two evaluations of dissipation
Contour lines $|g|$ = 1., .9, .8, ...
and locus of $z(\xi)$ for λ = 1.5, μ = .08
Coefficients α_1 = .6, α_2 = .6 , β = .625

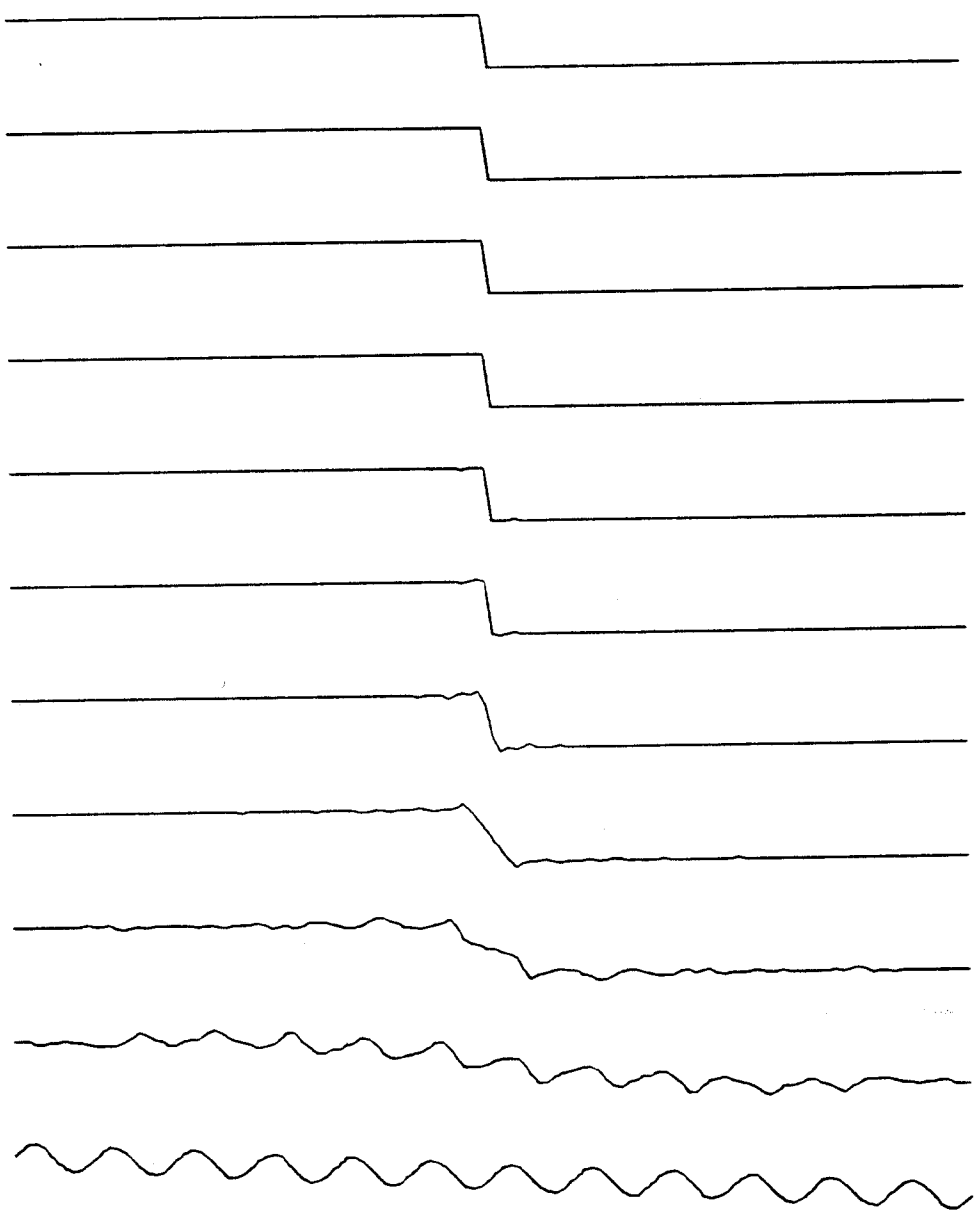

Figure 9(a)

Initial state and first 10 cycles in evolution
of Burger's equation (reading upwards)
Adaptive dissipation (scheme 1a)
128 cells 5 grids $\lambda = 2.0$

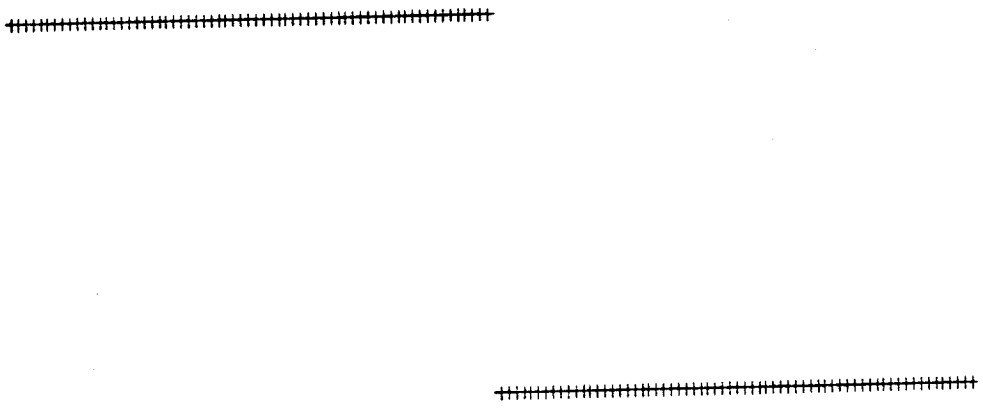

Figure 9(b)

Final State of Burger's equation
after 20 cycles of the multigrid scheme
Residual .5327 10-8

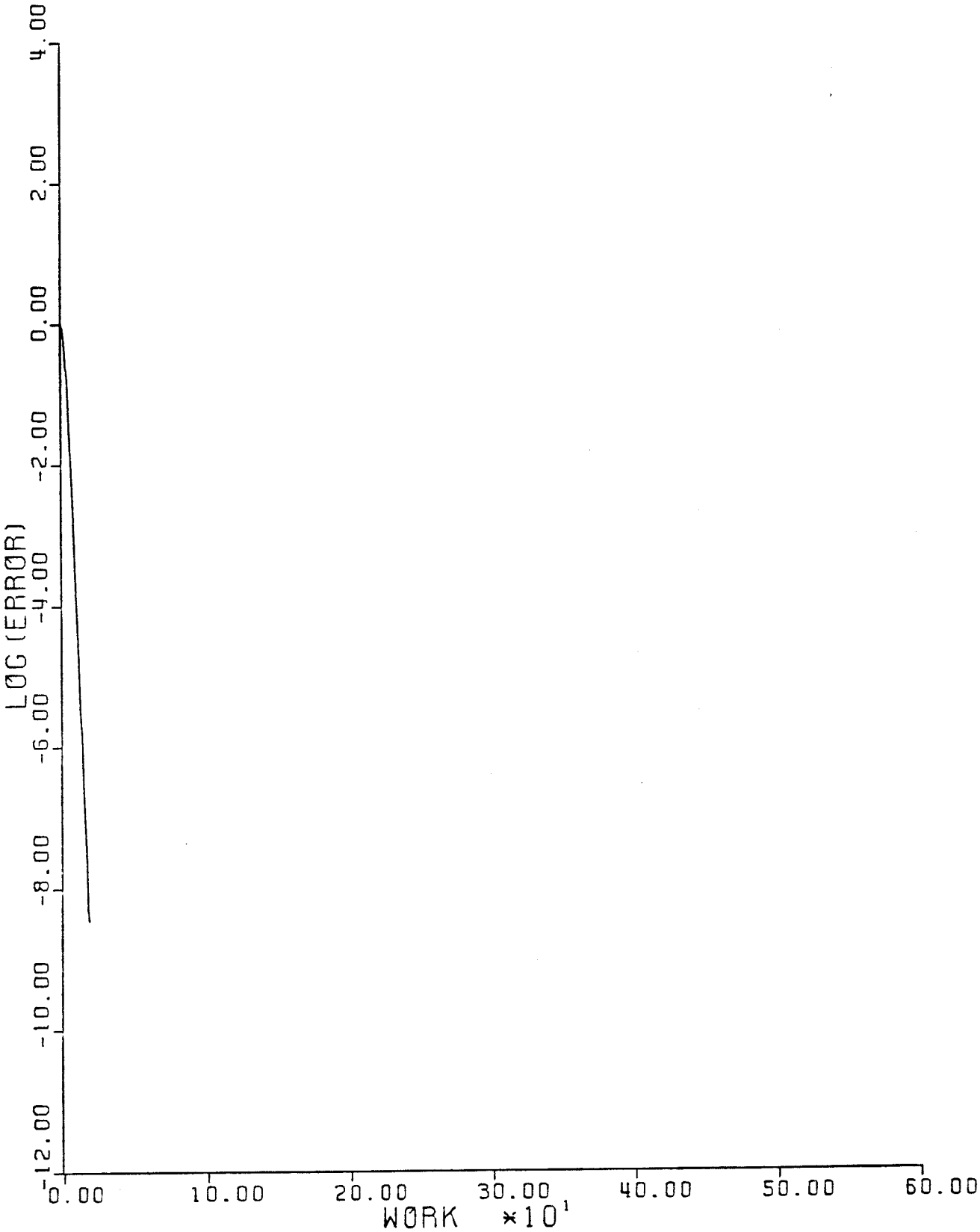

Figure 9(c)

Convergence history for Burger's equation
Adaptive Dissipation (scheme 1a)
128 cells 5 grids $\lambda = 2.0$
Mean rate of error reduction .3587 per cycle.

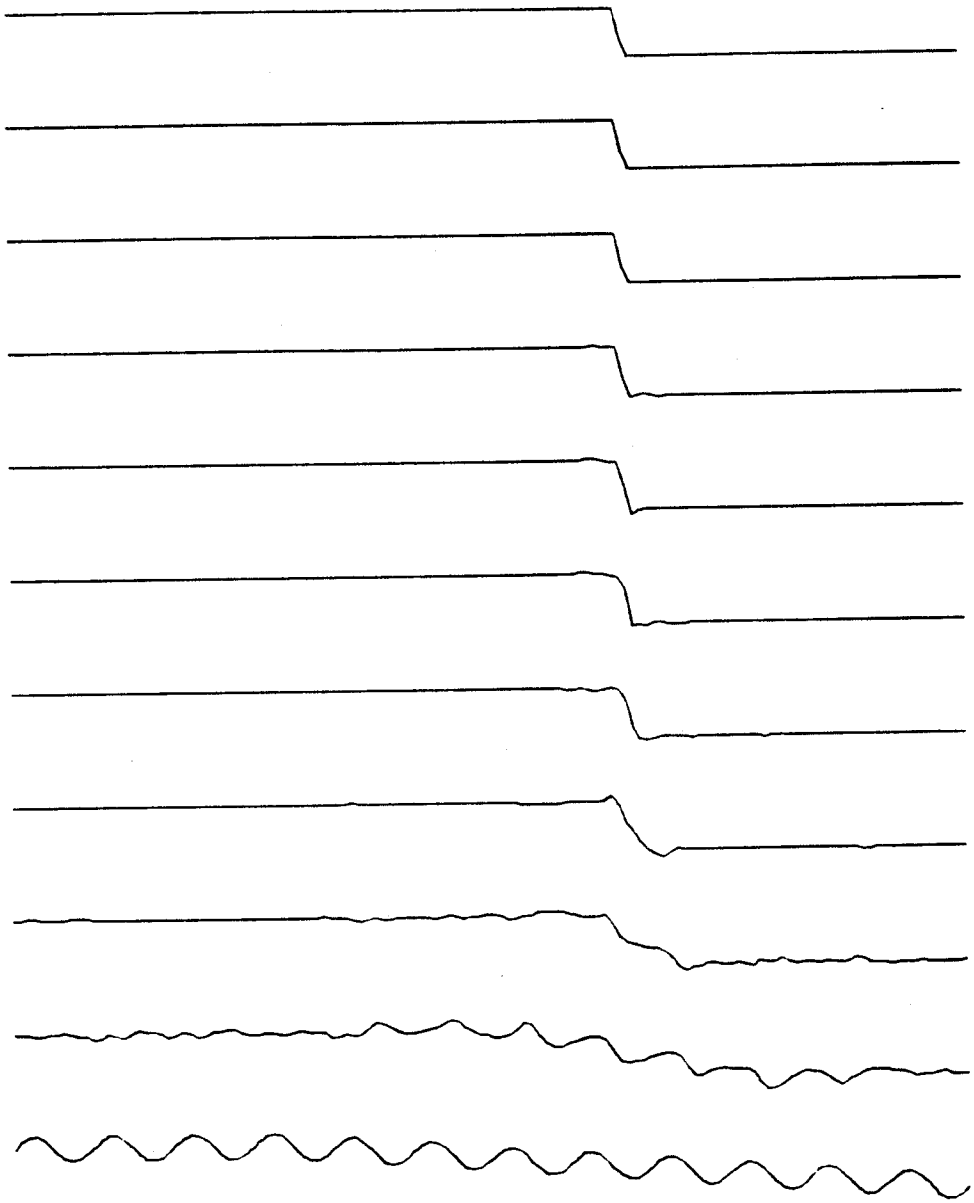

Figure 10(a)

Initial state and first 10 cycles in evolution
of Burger's equation (reading upwards)
Adaptive dissipation (scheme 1a)
128 cells 5 grids $\lambda = 2.0$

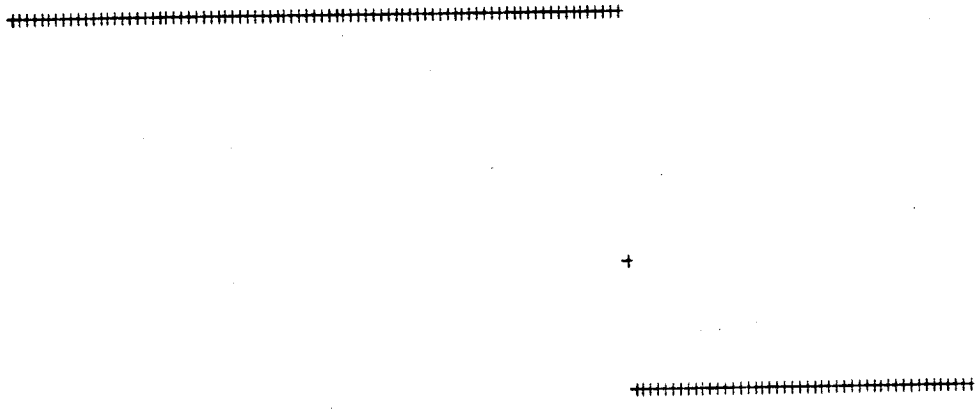

Figure 10(b)

Final State of Burger's equation
after 20 cycles of the multigrid scheme
Residual .2476 10^{-6}

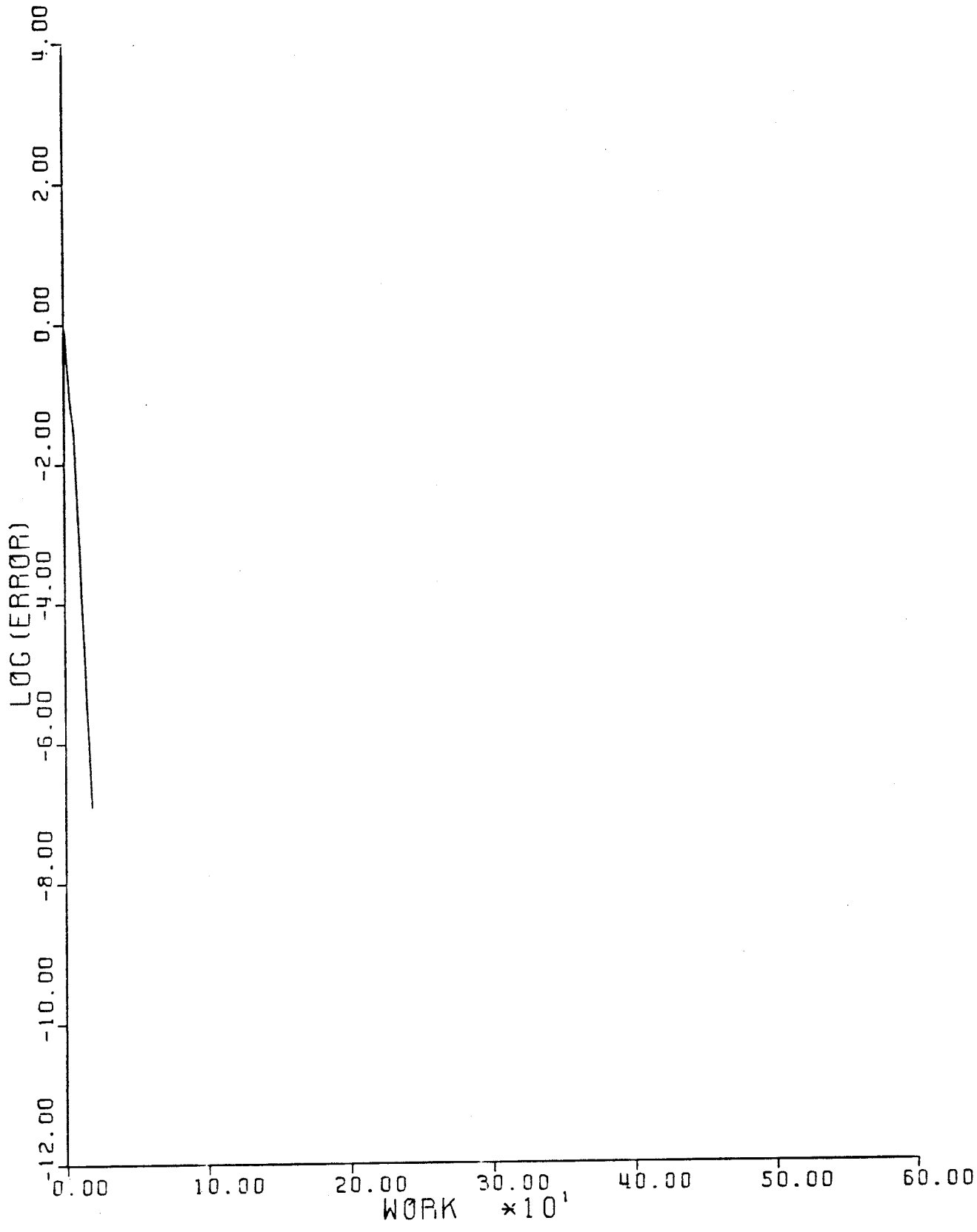

Figure 10(c)

Convergence history for Burger's equation
Adaptive Dissipation (scheme 1a)
128 cells 5 grids $\lambda = 2.0$
Mean rate of error convergence .4339 per cycle.

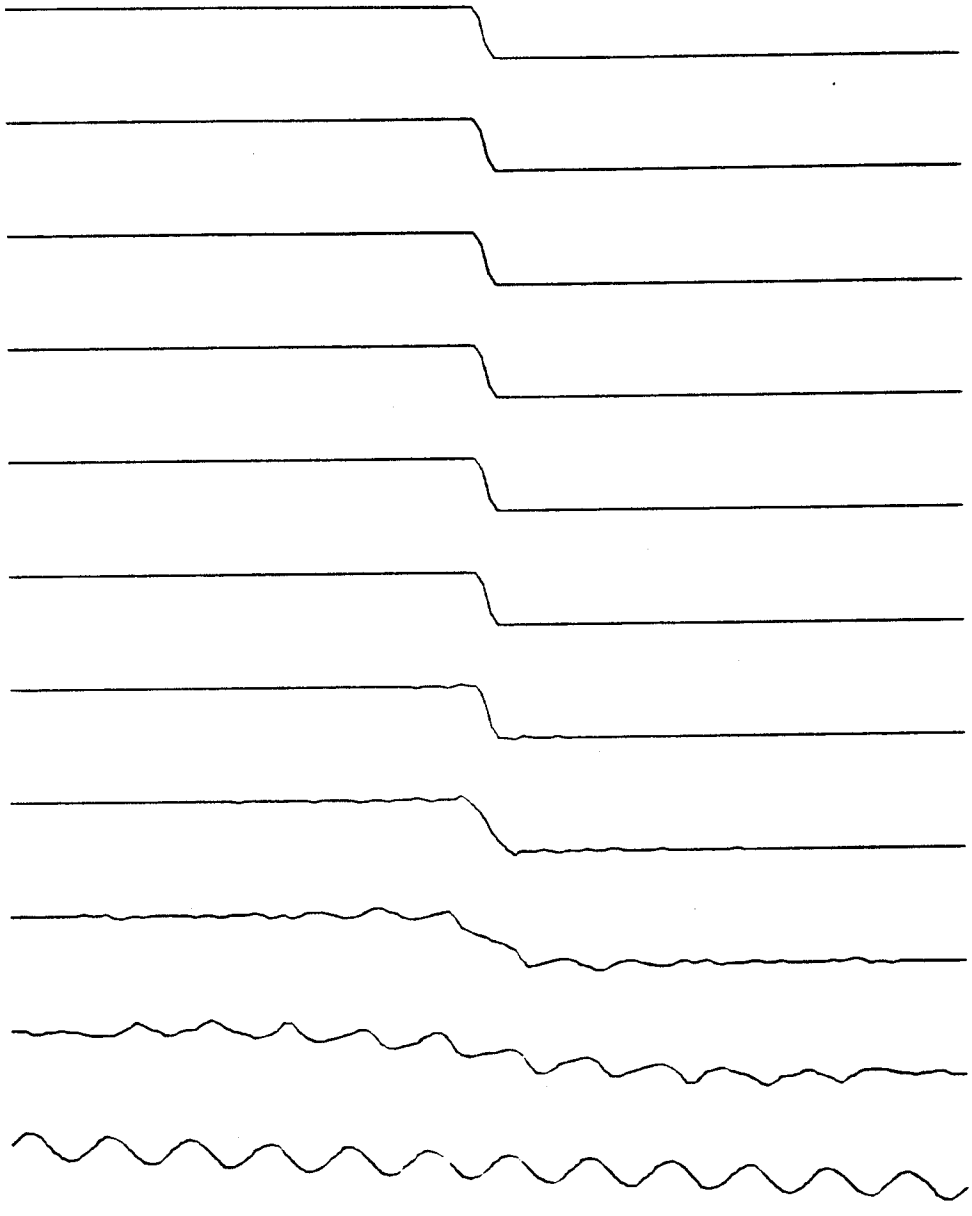

Figure 11(a)

Initial state and first 10 cycles in evolution
of Burger's equation (reading upwards)
Adaptive dissipation (scheme 1b)
128 cells 5 grids $\lambda = 2.0$

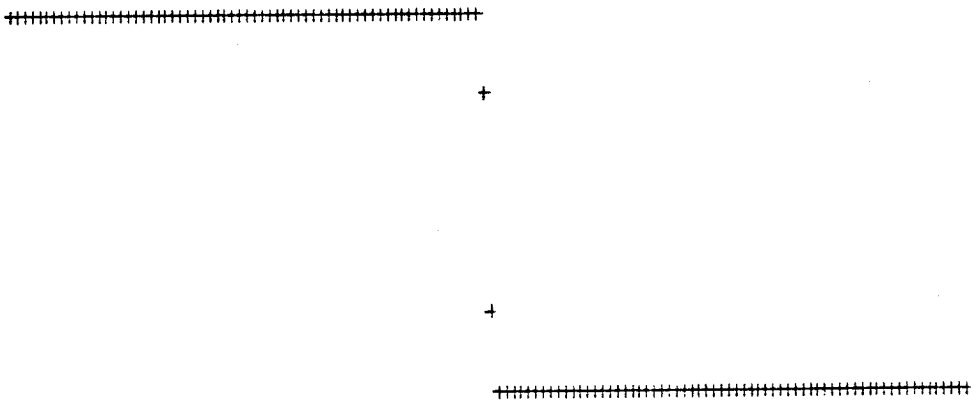

Figure 11(b)

Final State of Burger's equation
after 20 cycles of the multigrid scheme
Residual .9028 10^{-8}

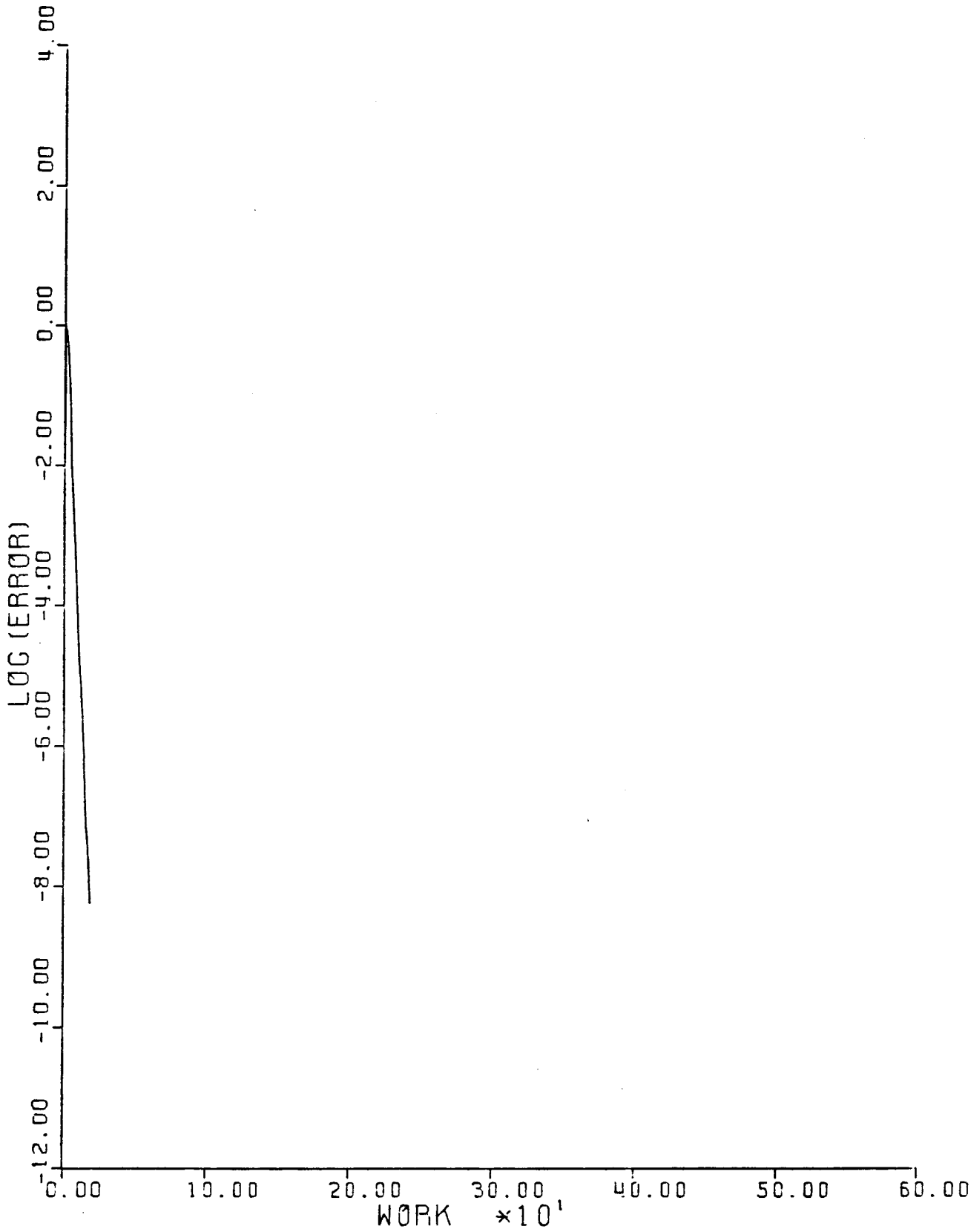

Figure 11(c)

Convergence history for Burger's equation
Adaptive Dissipation (scheme 1a)
128 cells 5 grids $\lambda = 2.0$
Mean rate of convergence .3688 per cycle.

11. Results for the Euler Equations

This section presents some typical results of multigrid calculations of the Euler equations for two-dimensional flow. The 5 stage scheme defined by equation (7.14) was used in all the examples, and residual averaging was also used to allow time steps corresponding to a Courant number of 7.5. Results are first presented for the standard scheme with adaptive dissipation as defined in Section 4.

The first example is the transonic flow past an NACA 64A410 airfoil at Mach .720 and an angle of attack $\alpha = 0^o$. Figure 6(a) shows the inner part of the grid, which contained 160 cells in the circumferential direction and 32 cells in the direction normal to the profile. The outer boundary of the grid is located at a distance of about 50 chords. Figure 6(b) displays the final pressure distribution in terms of the pressure coefficient

$$c_p = (p - p_\infty)/1/2\ \rho_\infty\ q_\infty^2$$

There is a moderately strong shock wave at about 60% of the chord on the upper surface. This result was obtained with 25 multigrid cycles on an 40 x 8 mesh, followed by 25 cycles on an 80 x 16 mesh, and finally 25 cycles on the 160 x 32 mesh. The calculation on the first mesh was started from an initial condition of uniform flow, and subsequently the result on each mesh was interpolated to provide the initial condition on the next mesh. 2 grid levels were used in the multigrid scheme on the 40 x 8 mesh, 3 grid leves on the 80 x 16 mesh, and 4 grid levels on the 160 x 32 mesh. Figure 6(c) shows the convergence history on the 160 x 32 mesh. Two measures are displayed. One curve shows the decay of the logarithm of the error (measured by the root mean square root of change of the density). The other curve shows the build up of the number of grid points

in the supersonic zone, which is a useful measure of global convergence. It can be seen that the flow field is already fully developed.

Two other typical examples are shown in the next two figures. Figure 13 shows the result for the NACA 0012 airfoil at Mach .8 and an angle of attack $\alpha = 1.25^{o}$, and Figure 14 shows the result for the Korn airfoil at Mach .75 and $\alpha = 0^{o}$. Each result was obtained with 50 cycles on an 80 x 16 mesh, followed by 50 cycles on a 160 x 32 mesh. This is sufficient for full development of the flow field. Such a calculation can be performed in 10 seconds with one processor of a Cray X/MP. The flow past the NACA 0012 airfoil contains a fairly strong shock wave on the upper surface, which is resolved in about four mesh cells, and a weak shock wave on the lower surface, which is quite smeared. The Korn airfoil is designed to be shock free at the given Mach number and angle of attack. The result of the Euler calculation is in close agreement with the result of the design calculation [32]. The drag should be zero in a shock free flow, and the calculated value of the drag coefficient CD = .0005 is an indication of the level of discretization error. Another measure of error is the entropy, which should also be zero. In this calculation the entropy, measured by

$$\frac{p}{\rho^{\gamma}} - \frac{p_{\infty}}{\rho_{\infty}^{\gamma}}$$

, is less than .001 everywhere in the flow field.

The final example shows the effect of replacing the scheme with adaptive dissipation by the TVD scheme for the case of the NACA 0012 airfoil at Mach .8 and $\alpha = 1.25^{o}$. The result is shown in Figure 15. It can be seen that sharper shock waves are obtained, with one interior cell. The entropy level ahead of the shock waves is much higher than in the calculation shown in Figure 12, however, and the stagnation enthalpy is no longer constant.

These results clearly demonstrate that the convergence of a time dependent hyperbolic system to a steady state can be substantially accelerated by the introduction of multiple grids. With the formulation here proposed, the steady state is entirely determined by the space discretization scheme on the fine grid. It is independent of both the time stepping scheme, and the discretization procedure used on the coarse grids. Either of these could be modified in any way which would improve the rate of convergence or reduce the computational effort. The existing scheme captures shocks fairly well using the adaptive dissipation of Section 4. The shock resolution is improved by the use of the TVD scheme of Section 5, at the expense of larger errors in the smooth part of the flow.

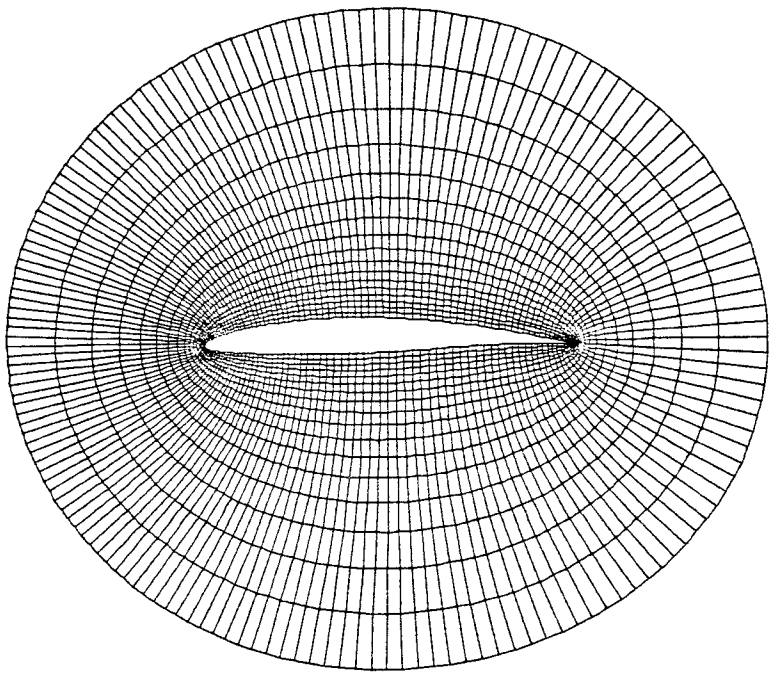

Figure 12(a)

Inner part of grid for NACA 64A410
160 x 32 cells

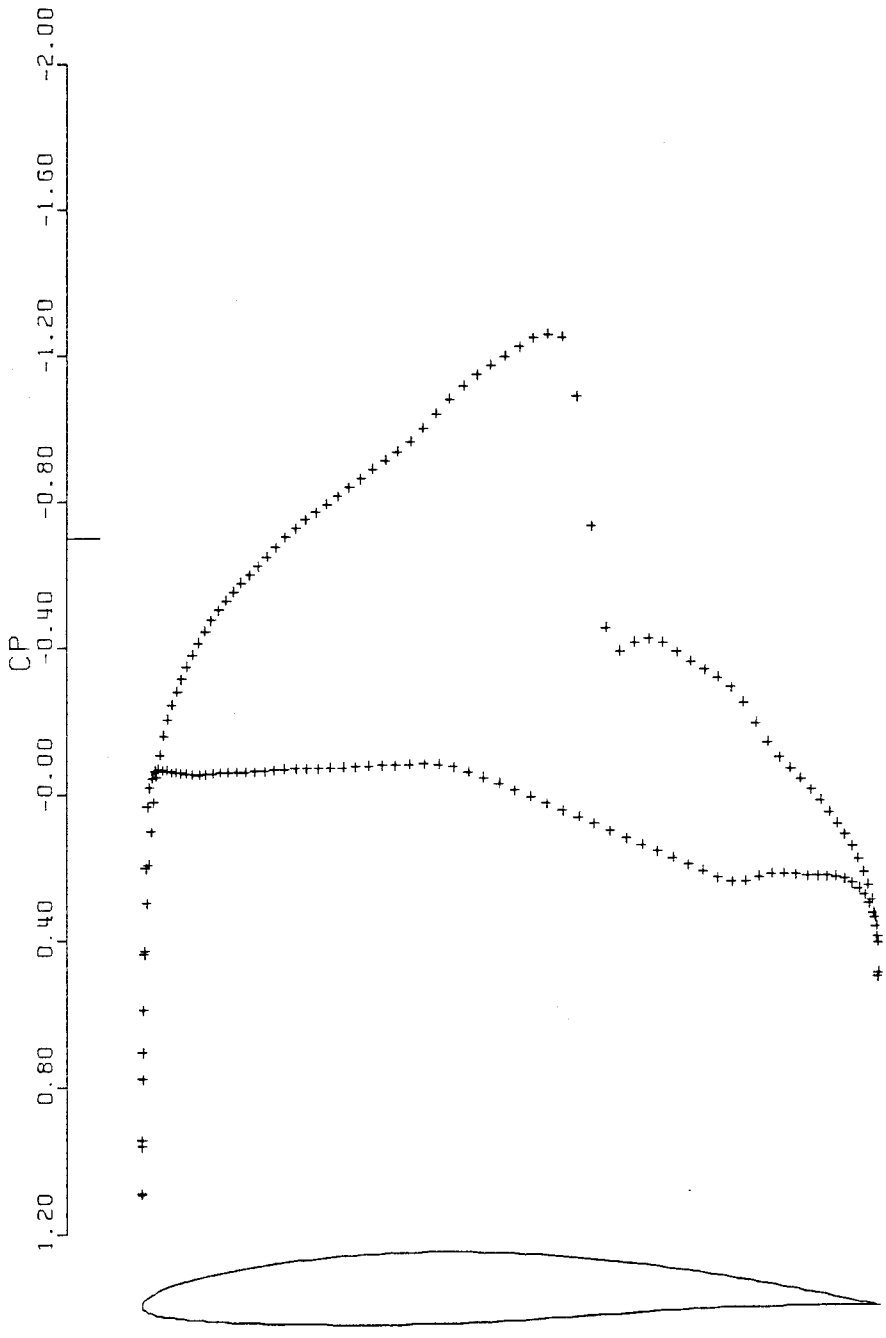

Figure 12(b)

Pressure distribution for NACA 64A410
Mach .450 α^{o}
CL .6292 CD .0036
160 x 32 grid 25 cycles Residual .248 10^{-3}

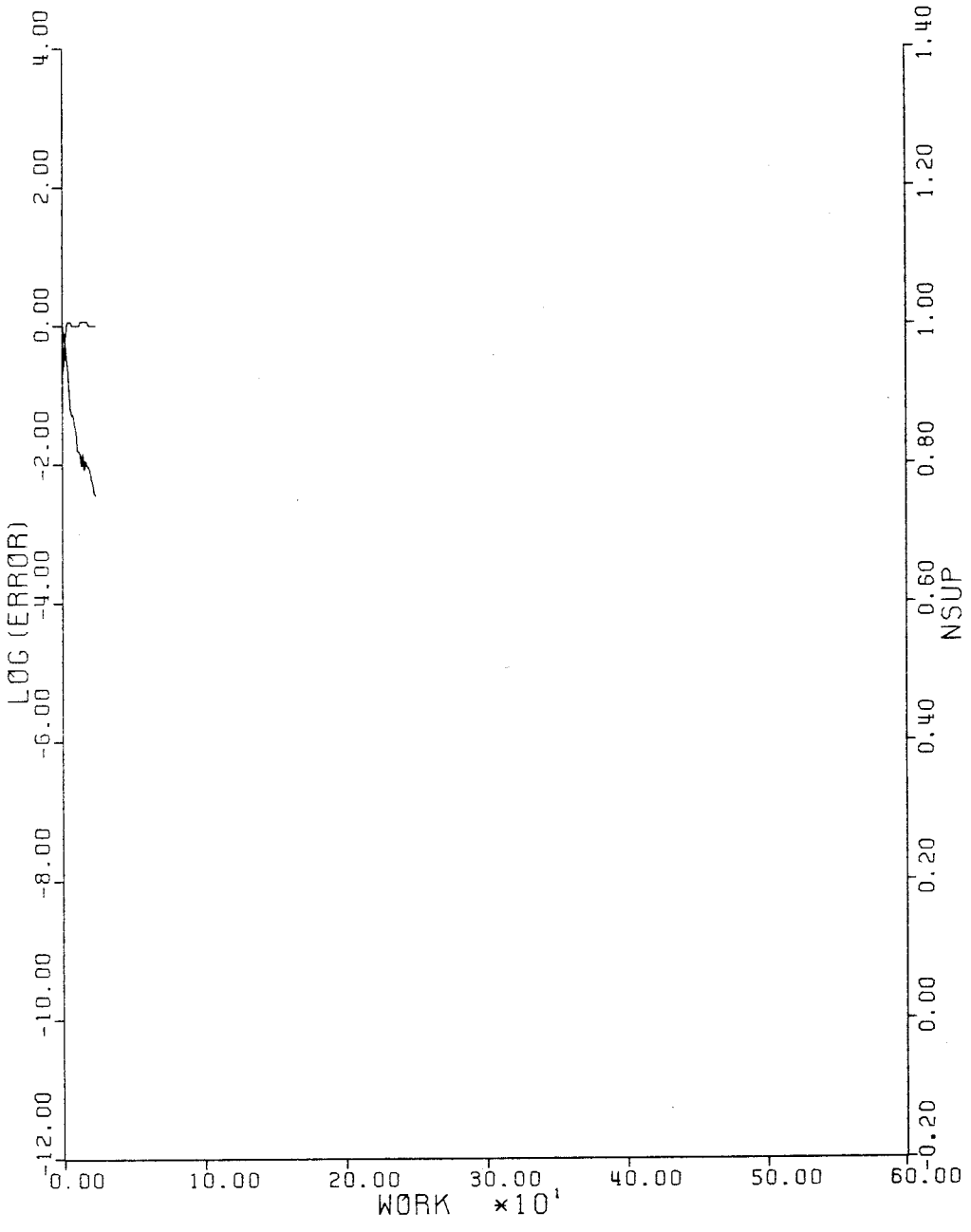

Figure 12(c)

Convergence history for NACA 64A410
Mach .720 $\alpha 0^{o}$
160 x 32 grid 25 cycles Residual .248 10^{-3}
Mean rate of convergence .7912 per cycle

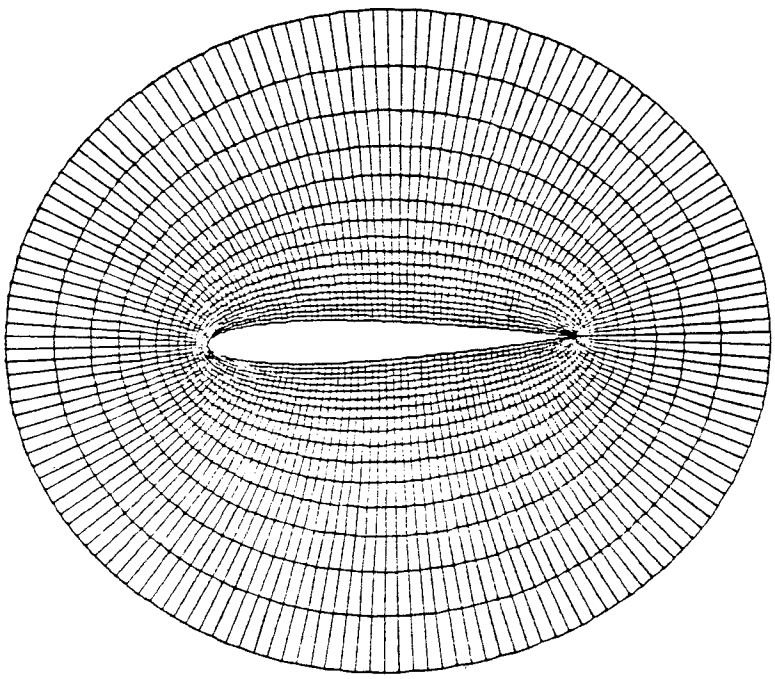

Figure 13(a)

Inner part of grid for NACA 0012
160 x 32 cells

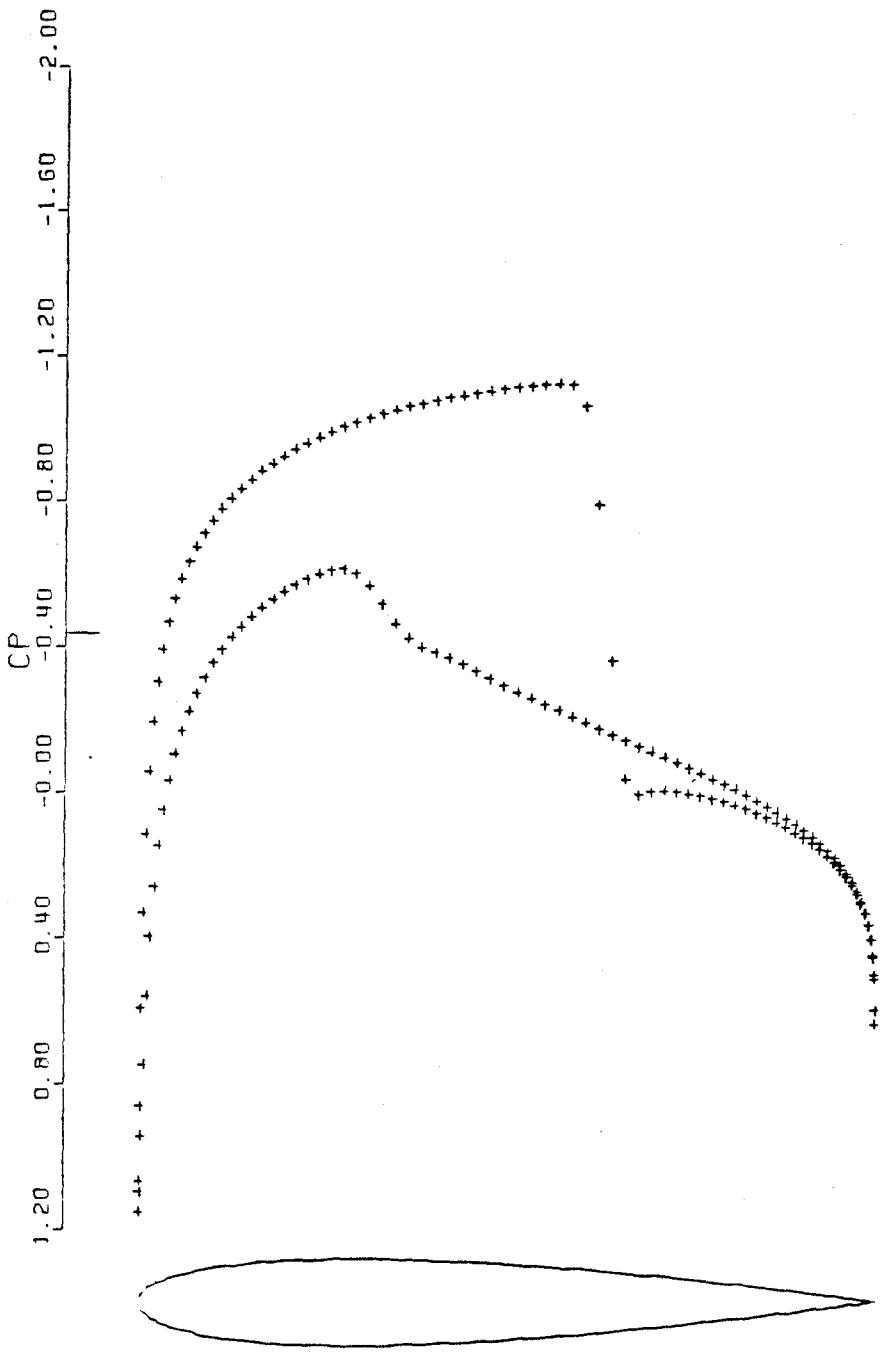

Figure 13(b)

Pressure distribution for NACA 0012
Mach .800 α 1.25°
CL .3504 CD .0227
160x32 grid 50 cycles Residual .152 10^{-3}

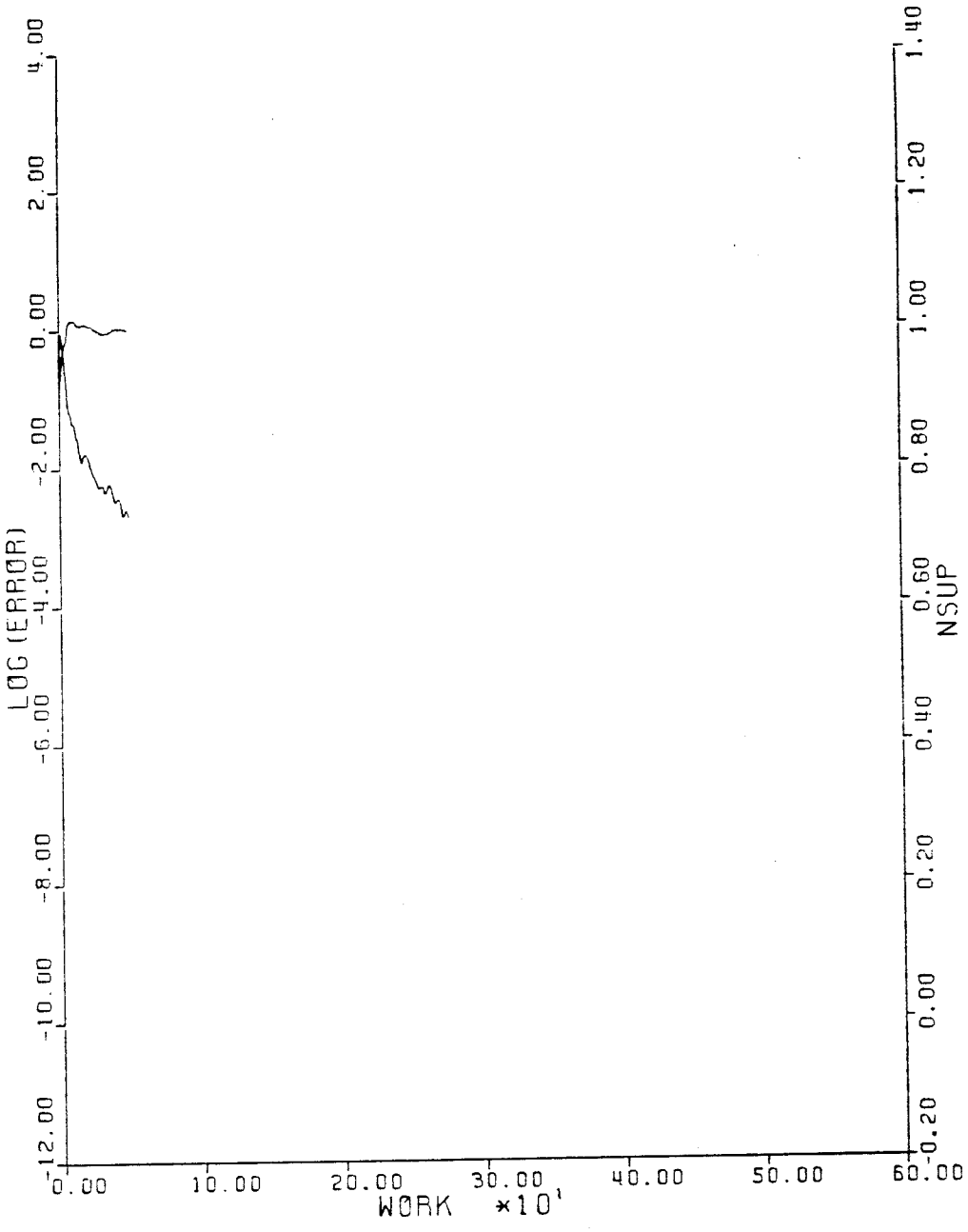

Figure 13(c)

Convergence history for NACA 0012
Mach .800 α 1.250
160 x 32 grid 50 cycles Residual .152 10^{-3}
Mean rate of convergence .8817 per cycle

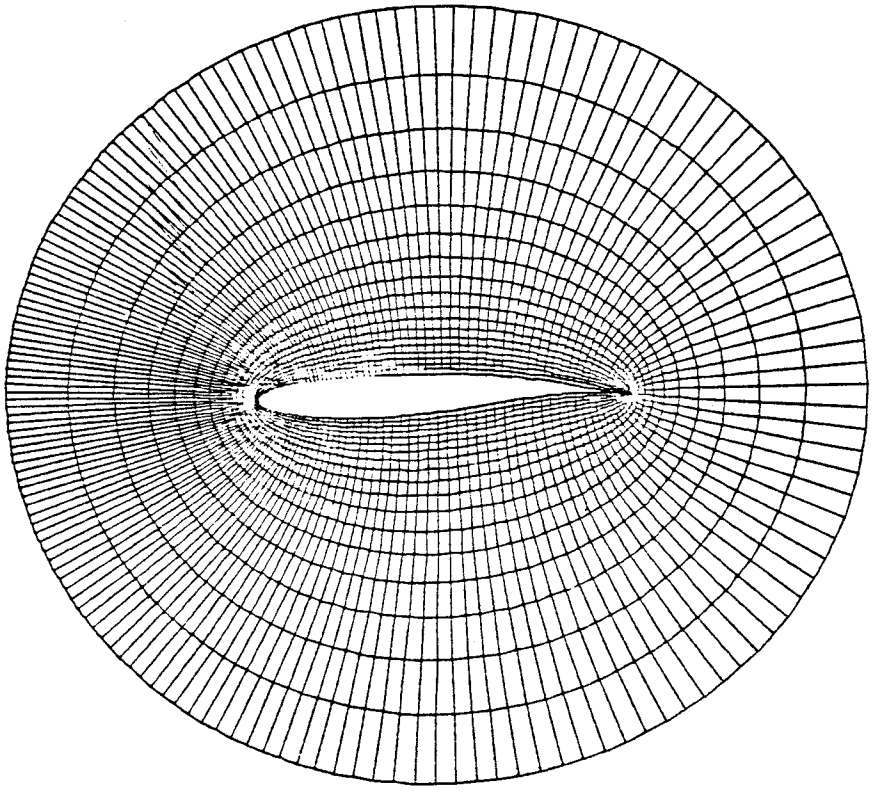

Figure 14(a)

Inner part of grid for Korn airfoil
160 x 32 cells

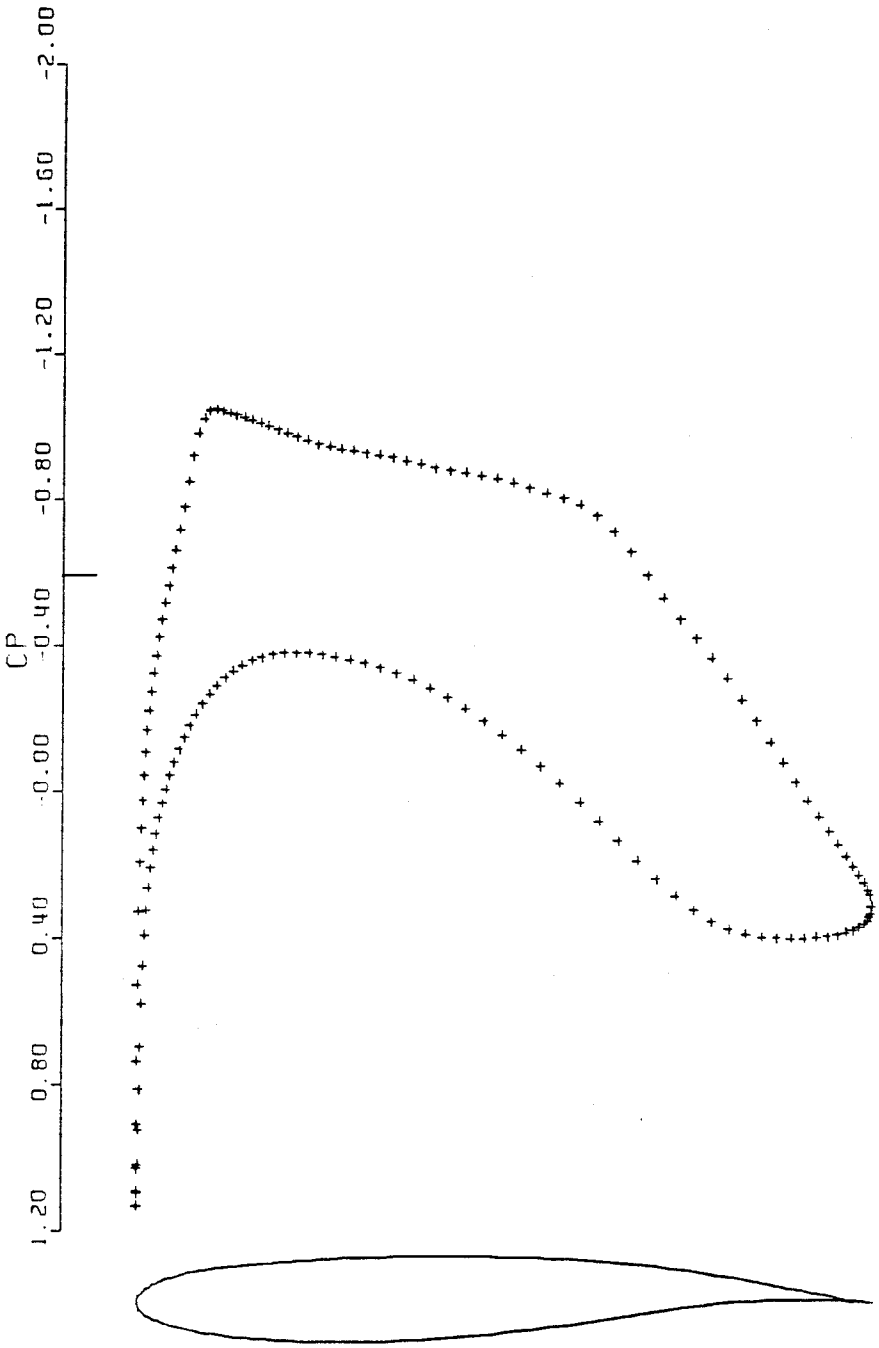

Figure 14(b)

Pressure distribution for Korn airfoil
Mach .750 α 0°
CL .6254 CD .0005
160 x 32 grid 50 cycles Residual .112 10^{-3}

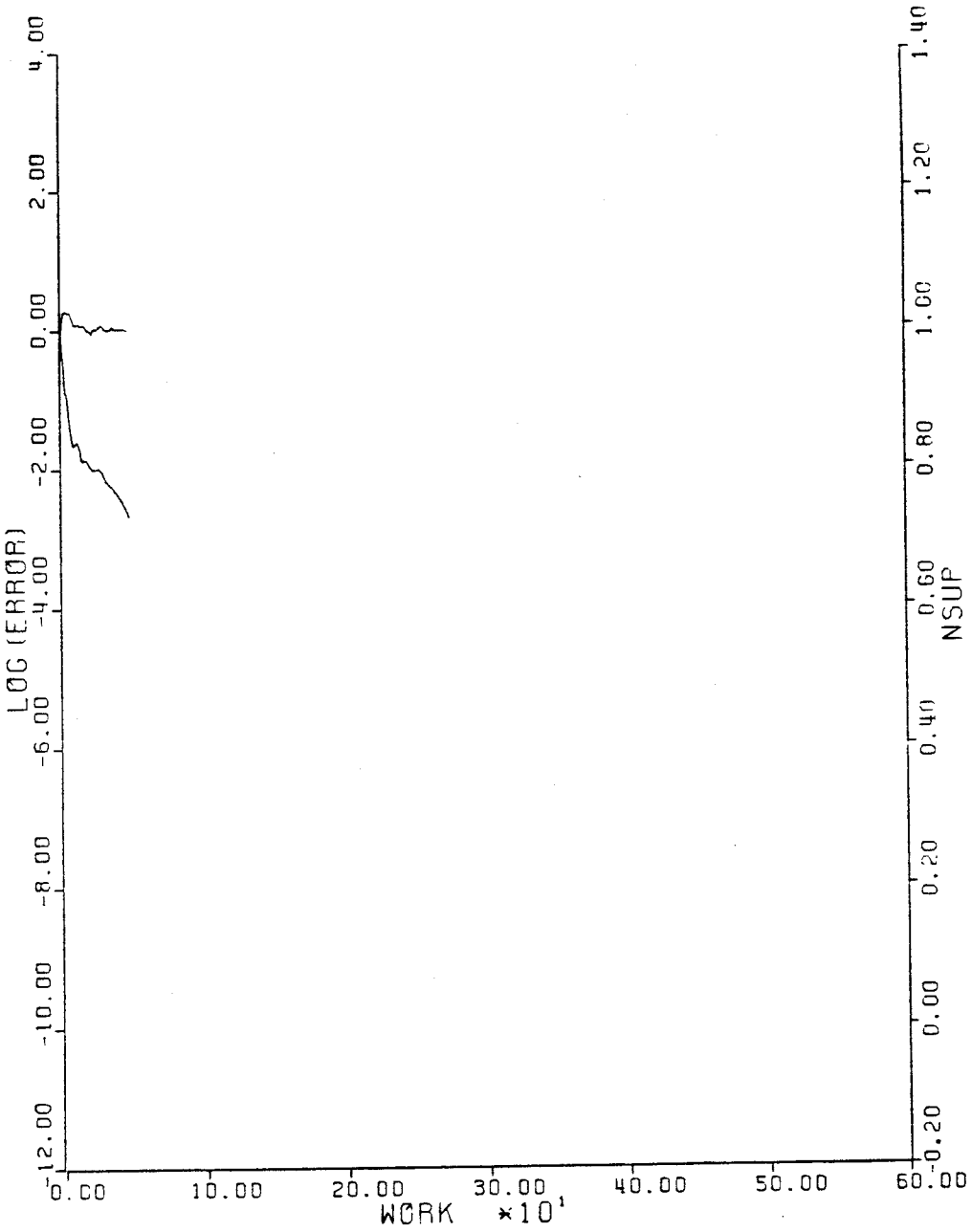

Figure 14(c)

Convergence history for Korn airfoil
Mach .750 α 0°
160 x 32 50 cycles Residual .112 10^{-3}
Mean rate of convergence .8820 per cycle

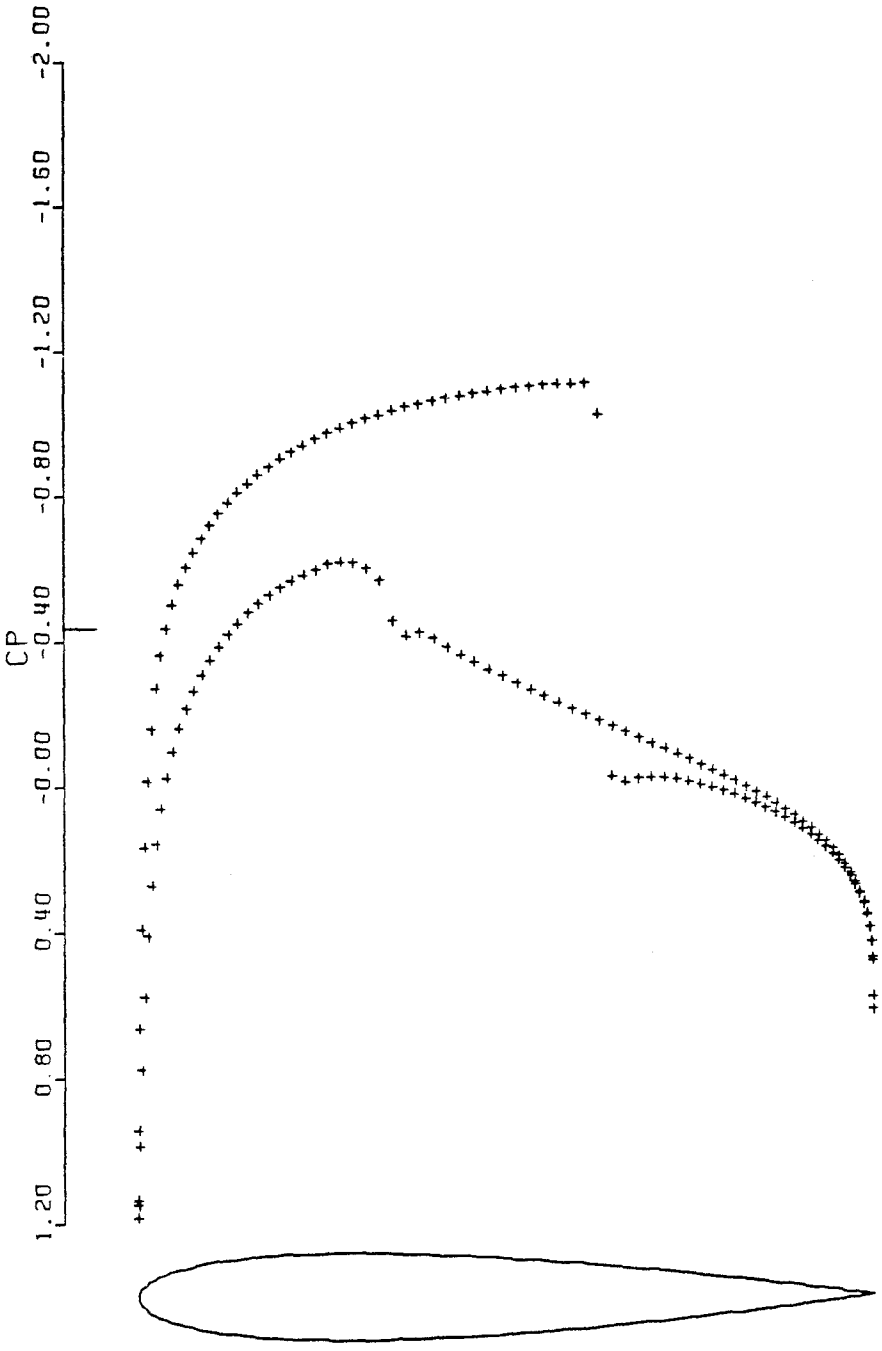

Figure 15

Pressure distribution for NACA 0012
Result using the TVD scheme.
Mach. .800 α 1.25°
CL .3349 CD .0262
160 x 32 grid 500 cycles Residual .869 10^{-4}

REFERENCES

1. Morawetz, C. S., "On the Non-Existence of Continuous Transonic Flows Past Profiles", Comm. Pure. Appl. Math., 9, 1956, pp. 45-48.

2. Jameson, Antony, "Transonic Aerofoil Calculations Using the Euler Equations", Proc. IMA Conference on Numerical Methods in edited by P. L. Roe, Academic Press, 1982, pp. 289-308.

3. Bristeau, M. O., Glowinski, R., Periaux, J., Perrier, P., Pironneau, O., and Poirier, G., "Transonic Flow Simulations by Finite Elements and Least Squares Methods", Proc. of 3rd International Conference on Finite Elements in Flow Problems, Banff, 1980, Vol. 1, edited by D. H. Norrie, pp. 11-29.

4. Lax, Peter and Wendroff, Burton, "Systems of Conservation Laws", Comm. Pure. Math., 13, 1960, pp. 217-237.

5. Harten, Amiram, Lax, Peter and van Leer, Brum, "On Upstream Differencing and Godunov Type Schemes for Hyperbolic Conservation Laws", SIAM Review, 25, 1983, pp. 35-61.

6. Osher, Stanley and Chakravarthy, Sukumar, "High Resolution Schemes and the Entropy Condition", ICASE Report NASA CR 172218, 1983.

7. Roe, P.L., "The Use of the Riemann Problem in Finite Difference Schemes", Proc. 7th International Conference on Numerical Methods in Fluid Dynamics, Stanford 1980, edited by W. C. Reynolds and R. W. MacCormack, Springer, 1981, pp. 354-359.

8. Roe, P.L., "Approximate Riemann Solvers, Parameter Vectors, and Difference Schemes", J. Computational Physics, 43, 1981, pp. 357-372.

9. Veiullot, J. P., and Viviand, H., "Methodes Pseudo-Instationnaire pour l'Calcul d' Ecoulements Transsoniques", ONERA Publication 1978-4, 1978.

10. Jameson, Antony, "Steady-State Solution of the Euler Equations for Transonic Flow", Proc. Symposium on Transonic, Shock and Multidimensional Flows, Madison, 1981, edited by R. E. Meyer, Academic Press, 1982, pp. 37-70.

11. Jameson, A., Schmidt, W., and Turkel, E., "Numerical Solution of the Euler Equations by Finite Volume Methods Using Runge-Kutta Time Stepping Schemes, AIAA Paper 81-1259, 1981.

12. Schmidt, W., and Jameson, A., "Recent Developments in Finite Volume Time Dependent Techniques for Two and Three Dimensional Transonic Flows", Von Karman Institute Lecture Series 1982-04, 1982.

13. Boris, J. P., and Book, D. L., "Flux Corrected Transport, 1, SHASTA, A Fluid Transport Algorithm that Works", J. Computational Physics, 11, 1973, pp. 38-69.

14. Zalesak, Stephen, "Fully Multidimensional Flux Corrected Transport Algorithm for Fluids", J. Computational Physics, 31, 1979, pp. 335-362.

15. Harten, A., "High Resolution Schemes for Hyperbolic Conservation Laws", New York University Report DOE/ER 03077-175, 1982.

16 Lax, P. D., "Hyperbolic Systems of Conservation Laws and the Mathematical Theory of Shock Waves", SIAM Regional Series on Applied Mathematics, 11, 1973.

17. Jameson, Antony, and Lax, Peter D., "Conditions for the Construction of Multi-Point Total Variation Diminishing Difference Schemes," Princeton University, Report MAE 1650, 1984.

18. Osher, S., "Riemann Solvers, The Entropy Condition, and Difference Approximations", To appear in SIAM Journal on Numerical Analysis.

19. Harten, A., Hyman, J. M., Lax, P.D., and Keyfitz, B., "On Finite Difference Approximations and Entropy Conditions for Shocks", Comm. Pure Appl. Math, 29, 1976, pp. 297-322.

20. Crandall, M., and Majda, A., "Monotone Difference Approximations for Scalar Conservation Laws", Math. Comp., 34, 1980, pp. 1-21.

21. Roe, P.L., "Some Contributions to the Modelling of Discontinuous Flows", Proc. AMS/SIAM Summer Seminar on Large Scale Computation in Fluid Mechanics, San Diego, 1983.

22. Sweby, P.K., "High Resolution Schemes Using Flux Limiters for Hyperbolic Conservation Laws", to appear in J. Computational Physics.

23. van Leer, Bram, "Towards the Ultimate Conservative Difference Scheme. II. Monotonicity and Conservation Combined in a Second Order Scheme," J. Computational Physics, 14, 1974, pp. 361-370.

24. Goodman, J. B., and Leveque, R. J., "On the Accuracy of Stable Schemes for 2-D Scalar Conservation Laws", to appear in Math. Comp.

25. Van der Houwen, "Construction of Integration Formulas for Initial Value Problems", North Holland, 1977.

26. Sonneveld, P., and van Leer, B., "Towards the Solution of Van der Houwen's Problem", to appear in Nieuw Archief voor Wiskunde.

27. Roe, P. L., and Pike, J., "Restructuring Jameson's Finite Volume Scheme for the Euler Equations", RAE Report, 1983.

28. Jameson, A., and Baker, T. J., "Solution of the Euler Equations for Complex Configurations", Proc. AIAA 6th Computational Fluid Dynamics Conference, Danvers, 1983, pp. 293-302.

29. Lerat, A., Sides, J., and Daru, V., "An Implicit Finite Volume Scheme for Solving the Euler Equations", Proc. 8th International Conference on

Numerical Methods in Fluid Dynamics, Aachen, 1982, edited by E. Krause, Springer, 1982, pp. 343-349.

30. Ni, R.H., "A Multiple Grid Scheme for Solving the Euler Equations", Proc. AIAA 5th Computational Fluid Dynamics Conference, Palo Alto, 1981, pp. 257-264.

31. Jameson, Antony, "Solution of the Euler Equations by a Multigrid Method", Applied Mathematics and Computation, 13, pp. 327-356.

32. Bauer, F., Garabedian, P., Korn, D., and Jameson, A., "Supercritical Wing Sections II, Springer, 1975.

ACKNOWLEDGEMENTS

This work has been carried out with the support of the Office of Naval Research, under Grant N00014-81-K-0379, and the NASA Langley Research Center, under Grant NAG-1-186. The method has been rather widely used, and many people have contributed to its improvement. Wolfgang Schmidt has been my principal collaborator in developing the method as a useful tool for aerodynamic analysis. More recently Tim Baker has assumed a key role in the extension of the method to treat complex three dimensional configurations. Manuel Salas made an important improvement in the accuracy of the prediction of lift. I have also benefited from continuing exchanges of ideas with Eli Turkel. Discussions with Stan Osher, Bram van Leer and Paul Woodward have been a great help to me in preparing Section 5, on TVD schemes.